

**The histone acetyltransferase CBP participates in regulating the DNA damage response through ATM after double-strand breaks**

RAMADAN, Wafaa S., AHMED, Samrein <<http://orcid.org/0000-0001-9773-645X>>, TALAAT, Iman M., LOZON, Lama, MOUFFAK, Soraya, GEMOLL, Timo, MANSOUR, Wael Y. and EL-AWADY, Raafat

Available from Sheffield Hallam University Research Archive (SHURA) at:

<https://shura.shu.ac.uk/35342/>

---

This document is the Published Version [VoR]

**Citation:**

RAMADAN, Wafaa S., AHMED, Samrein, TALAAT, Iman M., LOZON, Lama, MOUFFAK, Soraya, GEMOLL, Timo, MANSOUR, Wael Y. and EL-AWADY, Raafat (2025). The histone acetyltransferase CBP participates in regulating the DNA damage response through ATM after double-strand breaks. *Genome Biology*, 26 (1): 89. [Article]

---

**Copyright and re-use policy**

See <http://shura.shu.ac.uk/information.html>

RESEARCH

Open Access



# The histone acetyltransferase CBP participates in regulating the DNA damage response through ATM after double-strand breaks

Wafaa S. Ramadan<sup>1,2</sup>, Samrein B. M. Ahmed<sup>3</sup>, Iman M. Talaat<sup>1,2</sup>, Lama Lozon<sup>1,2</sup>, Soraya Mouffak<sup>1</sup>, Timo Gemoll<sup>4</sup>, Wael Y. Mansour<sup>5,6,7\*</sup> and Raafat El-Awady<sup>1,8\*</sup> 

<sup>†</sup>Wael Y. Mansour and Raafat El-Awady have shared last authorship.

\*Correspondence: [wmansour@uke.de](mailto:wmansour@uke.de); [relawady@sharjah.ac.ae](mailto:relawady@sharjah.ac.ae)

<sup>1</sup> Research Institute for Medical and Health Sciences, University of Sharjah, Sharjah, United Arab Emirates

<sup>5</sup> Department of Radiotherapy and Radiation Oncology, University Medical Center Hamburg-Eppendorf, Hamburg, Germany

Full list of author information is available at the end of the article

## Abstract

**Background:** Spatial and temporal control of DNA damage response pathways after DNA damage is crucial for maintenance of genomic stability. Ataxia telangiectasia mutated (ATM) protein plays a central role in DNA damage response pathways. The chain of events following induction of DNA damage that results in full activation of ATM is still evolving. Here we set out to explore the role of CREB-binding protein (CBP), a histone acetyltransferase (HAT), in DNA damage response, particularly in the ATM activation pathway.

**Results:** In response to DNA damage, CBP is stabilized and is recruited at sites of DNA double-strand breaks where it acetylates ATM and promotes its kinase activity. Cells deficient in CBP display an impairment in DNA double-strand break repair and high sensitivity to chemo- and radiotherapy. Importantly, re-expressing CBP's HAT domain in CBP-deficient cells restores the DNA repair capability, demonstrating the essential role of CBP's HAT domain in repairing DNA double-strand breaks.

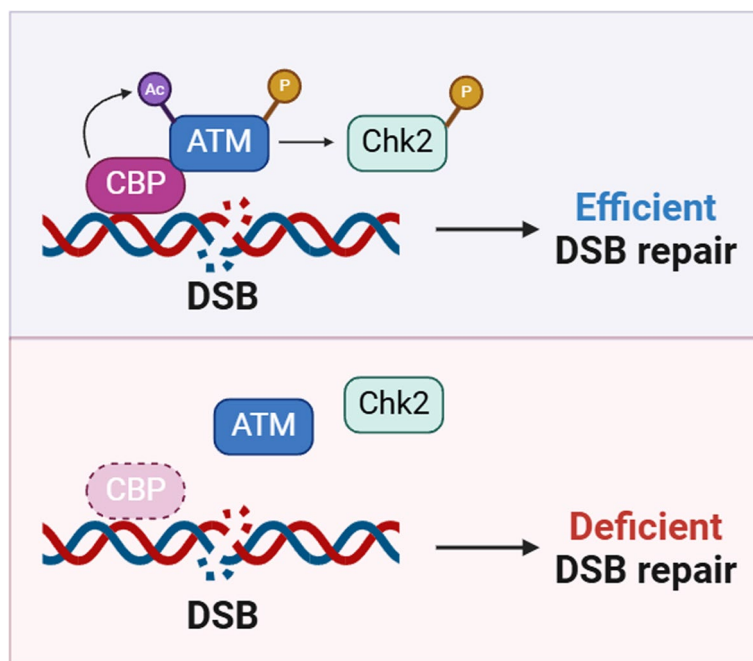
**Conclusions:** Together, our findings shed the light on CBP as a key participant in the ATM activation pathway and in the subsequent repair of DNA double-strand breaks, which may serve as a potential target to modulate the cellular response to DNA damaging agents in cancer.

**Keywords:** CBP, ATM, Histone acetyltransferase, DNA DSBs, DNA repair



© The Author(s) 2025. **Open Access** This article is licensed under a Creative Commons Attribution-NonCommercial-NoDerivatives 4.0 International License, which permits any non-commercial use, sharing, distribution and reproduction in any medium or format, as long as you give appropriate credit to the original author(s) and the source, provide a link to the Creative Commons licence, and indicate if you modified the licensed material. You do not have permission under this licence to share adapted material derived from this article or parts of it. The images or other third party material in this article are included in the article's Creative Commons licence, unless indicated otherwise in a credit line to the material. If material is not included in the article's Creative Commons licence and your intended use is not permitted by statutory regulation or exceeds the permitted use, you will need to obtain permission directly from the copyright holder. To view a copy of this licence, visit <http://creativecommons.org/licenses/by-nc-nd/4.0/>.

## Graphical Abstract



## Background

Genotoxic stress is a ubiquitous form of cellular stress that is caused by endogenous (e.g., reactive oxygen species) and exogenous agents (e.g., chemo- and radiotherapy), inducing DNA damage and genomic instability [1]. Cells counteract the induced DNA damage by utilizing highly conserved DNA damage response (DDR) pathways, which are indispensable surveillance networks for maintaining genomic integrity and stability. DDR has been envisioned as a cascade of signal transduction initiated by DNA damage sensors to activate transducers that passed down the signal to the effector proteins to execute the essential cellular functions such as cell cycle arrest, DNA repair, apoptosis, or cell senescence [2]. Among a variety of functionally diverse proteins in DDR machinery, Ataxia telangiectasia mutated (ATM) has been well recognized as the most upstream kinase which orchestrates a complex network of signaling events and triggers activation of several downstream targets such as Chk2, Chk1, 53BP1, and BRCA1, in response to DNA double-strand breaks (DSBs) [3]. Indeed, DNA DSBs are extremely cytotoxic and more difficult to repair compared to other types of DNA lesions. DSBs can be repaired by one of the two distinct pathways, homologous recombination (HR) and non-homologous end joining (NHEJ). HR repair pathway is highly accurate, which requires the homologous sister chromatid for ligation of DSB ends. It involves the MRN complex, CtIP, RAD51, and strand exchange to restore lost information [4], while NHEJ is an error-prone repair pathway, which involves the joining of DSB ends with minimal DNA processing. In NHEJ, Ku70/Ku80 heterodimers recruit DNA-PK to process DNA ends and ligate them with the XRCC4/Ligase IV complex. Both DSBs repair pathways are regulated by DDR kinases, including ATM, and are essential for maintaining genome

integrity [5]. Despite the vast volume of reports about ATM activation under DNA damage, the initiation of ATM activation after induction of DNA DSBs is still not fully understood. In addition, the requirement of MRN complex for ATM activation is still a matter of controversy [6, 7]. Recently, histone acetyltransferases (HATs) and histone deacetylases (HDACs) have emerged as new players in ATM signaling through regulating the level of ATM acetylation under DNA damage [8–11]. The acetylation of ATM is required for the induction of its kinase activity and so far, Tip60 is the only reported HAT that is involved in ATM acetylation. Later on, many studies showed that acetylation mediated by HATs is an important covalent modification which regulates the activity of many other DDR proteins, highlighting the crucial role of HATs in the DDR [3, 12].

HATs represent a large group of proteins that regulate many cellular processes by modifying the acetylation status of histone and non-histone proteins and by acting as transcriptional co-activators [13]. Among HAT family, CREB-binding protein (CBP) is localized in the nucleus and has been reported as an essential player in a wide array of critical processes underlying cellular activities such as cell growth, differentiation, apoptosis, cell cycle, and DNA repair. Recent observations indicate that CBP deregulation may disrupt cellular homeostasis; therefore, genetic alterations as well as functional dysregulation of CBP have been implicated in the pathogenesis of many human cancers including breast cancer [14–18]. Further studies have demonstrated the requirement of CBP for genotoxic stress response and for maintaining genome integrity [19–21]. The acetylation of p53 by CBP in response to DNA damage is commonly known to increase its transcriptional activity [22]. The contribution of CBP in DNA repair has been reported through its role in the recruitment of NHEJ factors to the sites of DNA damage and in the acetylation of PCNA to direct its degradation during nucleotide excision repair [23, 24]. Furthermore, the transcriptional activation properties of CBP through histone acetylation have been evolved to induce the transcription of two regulators of HR, BRCA1, and RAD51 [25]. Though previous reports have demonstrated the role of CBP in DNA repair pathways, the involvement of CBP in the initial events of activating DDR pathways and the potential of targeting CBP in breast cancer therapy remains poorly understood.

Here we show that CBP is recruited at sites of DNA damage and its stability is increased under DNA damage. Our findings suggest that CBP is involved in ATM acetylation that induces the activity of ATM and promotes DNA DSBs repair. We demonstrate that CBP depletion impairs the DNA repair capacity and subsequently increases the sensitivity of breast cancer cells to chemo- and radiotherapy. Thus, our findings reported here provide mechanistic insights into the way by which CBP is involved in DDR pathway and define CBP as an important player in the repair of DNA DSBs through regulating ATM activity under DNA damage.

## Results

### CBP protein is stabilized upon DNA damage and is recruited at sites of DSBs

First, we sought to investigate the role of CBP in DDR in breast cancer. To that end, we selected the luminal breast cancer cell lines (MCF7 and T47D) based on prior finding indicating that CBP is highly expressed in luminal subtypes [14]. The selection of these two cell lines was also based on their distinct p53 status, MCF7 cells harbor wild-type

p53 while T47D cells contain mutant p53, which is critical for DNA repair. CBP levels were subsequently measured in these cell lines after treatment with 5  $\mu$ M of Doxorubicin (DOX). Notably, CBP protein level was increased in a time-dependent manner in both MCF7 and T47D cells post-DOX treatment (Fig. 1a–c). Consequently, we observed also a time-dependent increase in the acetylation level of the CBP downstream target p53 at lysine 382. In order to test whether this effect is DOX-specific, we analyzed the effect of other DNA damaging agents including Cisplatin (CIS), Mitomycin C (MMC), and Etoposide (ETOP) on CBP protein levels. The immunoblotting analysis demonstrates a prominent increase in CBP level after ETOP similar to that after DOX and obviously modest increase after CIS or MMC treatment (Fig. 1d). The mRNA level of CBP did not increase following treatment with DOX (Additional file 1: Fig. S1a), indicating that the DNA damage-dependent regulation of CBP is post-transcriptional. To investigate this, we inhibited the protein synthesis in T47D cells using the protein synthesis inhibitor cycloheximide to measure the degradation rate of CBP after DNA damage by DOX or

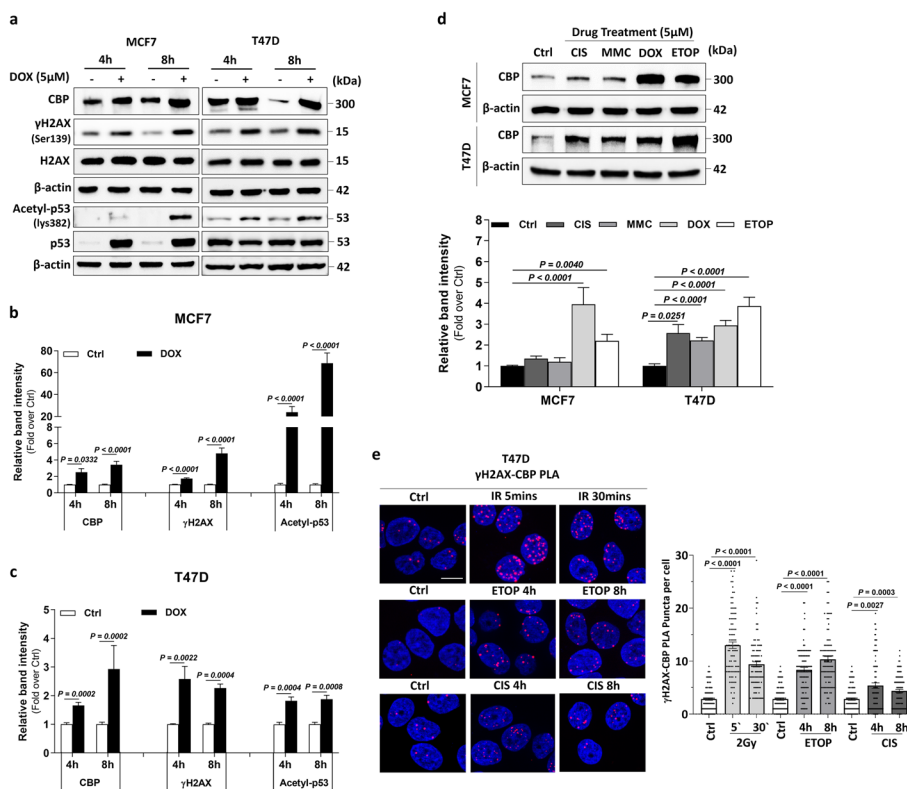


**Fig. 1** Modulation of CBP level and activity under DNA damage. **a** MCF7 and T47D cells were treated with 5  $\mu$ M of Doxorubicin (DOX) for 4 and 8 h, followed by immunoblotting analysis for CBP,  $\gamma$ H2AX, H2AX, acetyl-p53, and p53 proteins. **b, c** Graphs showing band quantifications for the indicated proteins in **c** MCF7 and **d** T47D cells, normalized to  $\beta$ -actin levels. **d** Upper panel: Immunoblot analysis for CBP expression in MCF7 and T47D cells treated with 5  $\mu$ M of Cisplatin (CIS), Mitomycin C (MMC), Doxorubicin (DOX), and Etoposide (ETOP) for 8 h. Lower panel: Band quantification of CBP expression, normalized to  $\beta$ -actin levels and presented as fold change relative to control samples. **e** Left panel: Proximity ligation assay (PLA) for CBP and  $\gamma$ H2AX colocalization (red) in T47D cells after 5 and 30 min of 2 Gy ionizing radiation (IR) or after 4 and 8 h treatment with 5  $\mu$ M of ETOP or CIS. DAPI staining (blue) marks the nucleus. Scale bar, 100  $\mu$ m. Right panel: Quantification of PLA signals from 100 cells. Data are represented as mean  $\pm$  SEM,  $n = 3$ .  $P < 0.05$  is considered significant, Mann–Whitney  $U$  test

ionizing radiation (IR). The results revealed that, after cycloheximide treatment, CBP degradation is less efficient following DNA damage induced by either DOX (5  $\mu$ M) or IR (10 Gray) compared to undamaged cells (Additional file 1: Fig. S1b-d). These findings suggest that the degradation rate of CBP may decrease following DNA damage, resulting in enhanced CBP stability.

Since CBP levels are increased specifically after treatment with IR, DOX, and ETOP, which mainly generate DNA DSBs, we therefore sought to test the involvement of CBP in the repair of such DNA damage. We firstly looked for the endogenous localization of CBP at sites of DNA DSBs in T47D cells. Similar to other DDR proteins as KU70/80, DNA-PKcs, and ligases [26, 27], CBP does not form foci upon DNA damage induction but instead displays a pan-nuclear distribution pattern (data not shown). Therefore, we used proximity ligation assay (PLA), which enables the in situ detection of endogenous protein interactions with exceptional specificity and sensitivity (Additional file 1: Fig. S2a-c) [28]. Using PLA, we reported that CBP colocalizes apparently with  $\gamma$ H2AX, a marker for DSBs, at 5 and 30 min after 2Gray (Gy) exposure and 4 and 8 h post-ETOP treatment; however, this colocalization occurred slightly after CIS treatment (Fig. 1e). Similar results of CBP recruitment at DNA damage sites were observed with MCF7 cells following IR (Additional file 1: Fig. S2d). Furthermore, PLA and co-immunoprecipitation experiments demonstrated an enhanced interaction between CBP and 53BP1, a downstream effector of  $\gamma$ H2AX, following DNA damage induction (Additional file 1: Fig. S2e, f), further supporting the recruitment of CBP at DSB sites. Collectively, these results demonstrate that CBP is more stabilized upon DNA damage and mainly recruited at DNA DSB sites.

### **CBP downregulation impairs DNA DSB repair**

To evaluate the functional importance of CBP in DSB repair, we efficiently depleted CBP using siRNA in both MCF7 and T47D cells (Additional file 1: Fig. S3a) and monitored the phosphorylation of H2AX at S139 ( $\gamma$ H2AX). CBP depletion significantly increased the number of  $\gamma$ H2AX foci detected at the 8-h time-point after DOX treatment in both cell lines, indicating a role for CBP in repairing DSBs (Fig. 2a). This data was recapitulated in T47D cells after irradiation with 2 Gy. We observed no change in the number of  $\gamma$ H2AX foci at 1 h post-2 Gy in CBP-depleted T47D cells compared to their wild-type counterparts. However, an increased number of residual  $\gamma$ H2AX foci at 24 h post-2 Gy were demonstrated in CBP-knockdown cells (Additional file 1: Fig. S3b). In order to confirm that the detected  $\gamma$ H2AX foci represent open DNA ends rather than a delay in H2AX dephosphorylation, physically opened DSBs were monitored using a neutral comet assay in CBP-depleted MCF7 or T47D cells after DOX treatment. Results revealed that the tail moments of CBP-depleted cells were markedly higher than those of control cells after 8 h of DOX treatment (Fig. 2b; Additional file 1: Fig. S3c). Additionally, the length and intensity of the comet were significantly higher in CBP-depleted cells compared to CBP-proficient cells after 6 h of drug removal and persisting at the same level up to 12 h, indicating compromised repair in CBP-deficient cells. Consistently, the clonogenic cell survival assay showed that CBP-depleted T47D or MCF7 cells exhibited

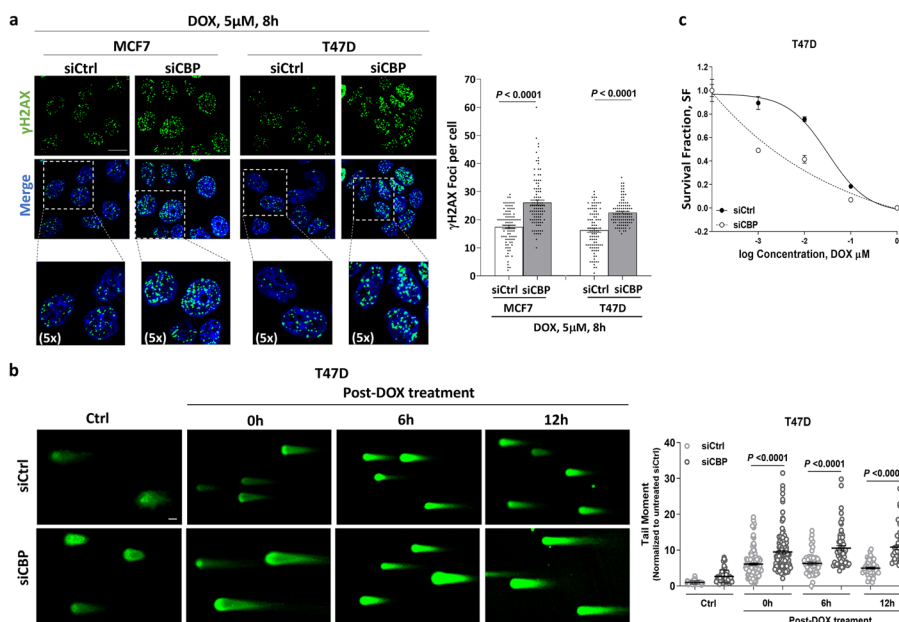


**Fig. 2** CBP depletion impairs DNA double-strand breaks repair in MCF7 and T47D cells. **a** Left panel: Immunofluorescence of γH2AX (green), merged with DAPI staining (blue) of nuclei, after 8 h treatment with Doxorubicin (DOX) in MCF7 and T47D cells transiently transfected with negative control (siCtrl) or CBP siRNA. Scale bar, 100 μm. Right panel: Average number of γH2AX foci per cell from 100 cells. **b** Left panel: Comet assay images showing DNA double-strand breaks repair kinetics following DOX removal in T47D cells transfected with the indicated siRNAs. Scale bar, 50 μm. Right panel: Quantification of the neutral comet assay by tail moment at 0, 6, and 12 h post-DOX incubation in T47D cells, from 50 cells. **c** Colony formation assay in T47D cells transfected with siCtrl or siCBP for 48 h and treated with the indicated concentrations of DOX. Data are represented as mean ± SEM,  $n = 3$ .  $P < 0.05$  is considered significant, Mann–Whitney  $U$  test

higher sensitivity to DOX than cells transfected with control siRNA (Fig. 2c; Additional file 1: Fig. S3d).

To further support our finding, we utilized CRISPR-Cas9 technology to generate CBP knockout (KO) cells. Six different CBP KO clones were generated, exhibiting varying levels of DDR kinase, ATM (Additional file 1: Fig. S4). To exclude the effect of variation in ATM levels, we selected two CBP KO cells with distinct ATM expression levels to further recapitulated our data on CBP’s involvement in DNA repair (Additional file 1: Fig. S5a). Although there was no difference in the number of γH2AX and 53BP1 foci (DSB marker) at 1 h post-2 Gy, the number of γH2AX and 53BP1 foci was significantly higher at 24 h post-2 Gy in CBP KO T47D cells compared to their wild-type counterparts (Additional file 1: Fig. S5b). Using the comet assay, the tail moments of CBP KO sublines were greater than those of wild-type cells after 6 and 12 h of DOX removal, indicating impaired DSB repair in CBP KO cells (Additional file 1: Fig. S5c). Additionally, the clonogenic cell survival assay showed increased sensitivity of CBP KO cells to various concentrations of DOX compared to parental T47D cells (Additional file 1: Fig. S5d). Ultimately, impaired ATM and Chk2 phosphorylation were observed in CBP KO cells after DOX or ETOP treatment (Additional file 1: Fig. S5e-g). Taken together, these results indicate that CBP contributes to the repair of DNA DSBs.

**CBP is involved in ATM activation in response to DNA damage**

HATs have been linked to ATM-dependent DNA damage signaling [8–10]. It is therefore plausible to suggest that the HAT CBP might be involved in DNA DSB repair by regulating ATM activity. To test this possibility, we first investigated the potential effect of CBP knockdown on DOX-induced ATM phosphorylation at S1981 (Fig. 3a). SiRNA-mediated CBP silencing decreased the level of DOX-induced p53 acetylation in MCF7 and T47D cells (Fig. 3c, e). Strikingly, ATM phosphorylation was impaired in CBP-knockdown MCF7 and T47D cells after DOX treatment (Fig. 3a, b, d). DNA damage-induced p-ATM foci were dramatically reduced in CBP-depleted MCF7 and T47D cells upon DOX treatment (Fig. 3f). The phosphorylation of the ATM downstream proteins, Chk2 at Thr68 and p53 at S15, was reduced in T47D cells (Fig. 3d, e) and consequently the expression of p21 was decreased. Similar results were obtained in another breast cancer

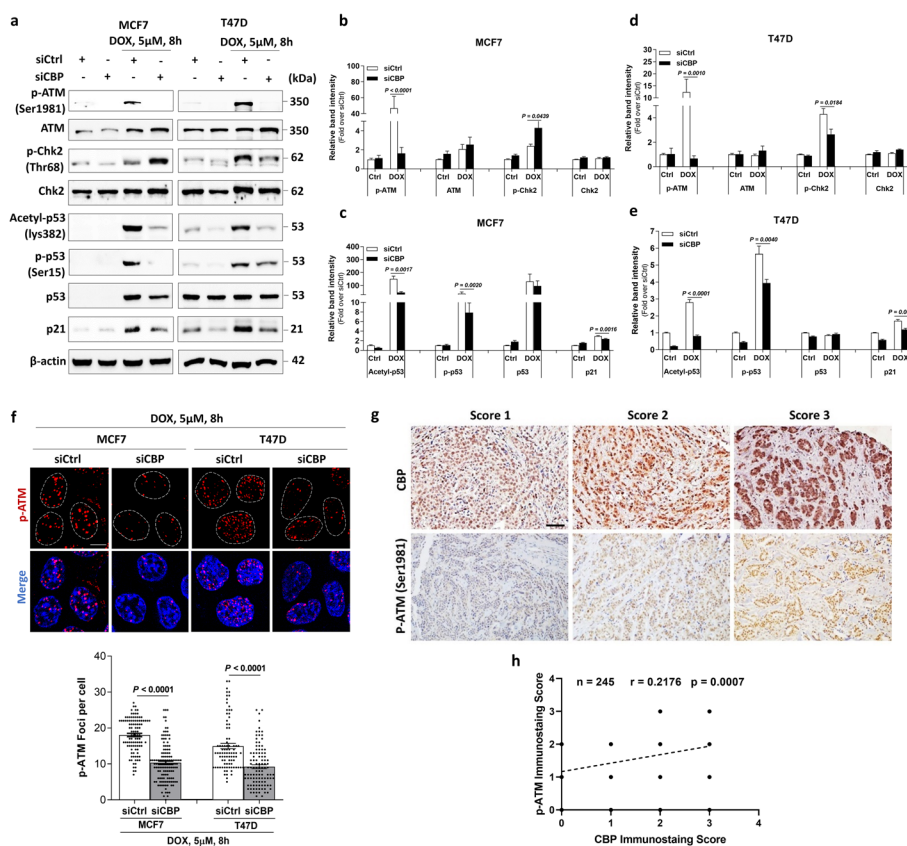


**Fig. 3** The effect of CBP depletion on the phosphorylation of ATM under DNA damage. **a** Immunoblotting analysis of p-ATM, ATM, p-Chk2, Chk2, acetyl-p53, p-p53, p53, and p21. Levels of the indicated proteins were detected in whole-cell extracts from MCF7 and T47D cells transfected with the indicated siRNAs followed by Doxorubicin (DOX) treatment. **b–e** Quantification of band intensities for indicated proteins normalized to the corresponding untreated siCtrl condition. **f** Upper panel: Representative images showing the formation of DOX-induced p-ATM foci (red) and merged with DAPI (blue) staining of nuclei in MCF7 and T47D cells transfected with negative control (siCtrl) or CBP siRNA. Scale bar, 100  $\mu$ m. Lower panel: The average number of p-ATM nuclear foci per cells from 100 cells. Data are represented as mean  $\pm$  SEM,  $n = 3$ .  $P < 0.05$  is considered significant, Mann–Whitney  $U$  test. **g** Representative images of CBP and p-ATM immunohistochemical staining in breast tissue samples. Immunostaining scores in tumor tissues are shown. Scale bar, 100  $\mu$ m. **h** Correlation analysis between CBP and ATM expression in 245 clinical breast cancer samples. Pearson’s correlation coefficient “ $r$ ” with the corresponding  $P$  value is shown

cell line, MDA-MB-231 cells (Additional file 1: Fig. S6a, b). Surprisingly, an increase in p-Chk2 levels was observed in CBP-depleted MCF7 cells after DOX treatment (Fig. 3b). This effect appears to be dependent on the p53 status of breast cancer cells. MCF7 cells express wild-type p53, while T47D and MDA-MB-231 cells harbor p53 mutations. Therefore, it seems that the level of p-Chk2 is maintained high, independent of p-ATM, to sustain the G1 arrest in CBP-depleted p53-wild-type MCF7 cells after DOX-induced DNA damage [29, 30]. These findings establish the pivotal function of CBP in promoting the activation of ATM and its downstream players in response to DNA damage in breast cancer cells. Consistent with this, further testing of the ATR/Chk1 axis revealed no significant changes upon CBP downregulation (Additional file 1: Fig. S6c, d).

To further substantiate the association of CBP and ATM phosphorylation, we evaluated the levels of CBP expression and p-ATM in breast cancer tissues by immunohistochemical staining (Fig. 3g). We observed a positive correlation between CBP expression and ATM phosphorylation in breast cancer specimens ( $p = 0.0007$ ) (Fig. 3h). Since our data demonstrated that CBP expression is mainly induced by DSBs and to a lesser extent by replication-associated damage (e.g., after CIS and MMC treatments), the correlation between CBP and p-ATM signals in patient tissues is not a strong, as the detected p-ATM signal in these tissues primarily reflects endogenous DNA damage arising from replication-associated damage.

#### **Involvement of CBP in DNA DSB repair is ATM-dependent**

The above results indicate an ATM-dependent role of CBP in DSB repair. To address this issue, ATM was inhibited by pre-treatment with the ATM inhibitor (ATMi) KU55933 (2.5 or 5  $\mu\text{M}$ ) for 2 h before IR in CBP-depleted T47D cells and  $\gamma\text{H2AX}$  and 53BP1 foci were then monitored at 1 and 24 h post-IR (Fig. 4a). Again, CBP-depleted cells showed more residual  $\gamma\text{H2AX}$  and 53BP1 foci at 24 h post-IR compared to non-depleted cells. However, no further increase in the residual foci was observed upon pre-treating CBP-depleted cells with 2.5 or 5  $\mu\text{M}$  of KU55933 (Fig. 4a; Additional file 1: Fig. S7a). Consistently, no significant differences were found in the tail moment of CBP-depleted T47D cells with and without treatment with 5  $\mu\text{M}$  of ATMi 24 h post-IR (Fig. 4b). This data was further recapitulated in the previously described ATM-deficient SKX cells, which were established from a biopsy obtained from a head and neck cancer patient [31]. CBP depletion did not further increase the number of residual  $\gamma\text{H2AX}$  and 53BP1 foci 24 h post-2 Gy in SKX cells (Additional file 1: Fig. S7b, c). CBP-downregulated T47D cells displayed increased sensitivity to IR compared to CBP-proficient cells. Pre-treatment with 2.5  $\mu\text{M}$  of KU55933 did not further increase the radiosensitivity of CBP-depleted cells (Fig. 4c); however, a slight increase was observed after treatment with 5  $\mu\text{M}$  of ATMi (Fig. 4c). Importantly, the radiosensitivity of ATM-deficient SKX cells was not affected by CBP downregulation (Fig. 4d). Together, these results indicate that CBP mediates the response to DNA damage primarily through ATM and provide evidence of an ATM deficient phenotype in CBP-depleted cells.

#### **The role of CBP in DNA damage response is independent on estrogen receptor status**

CBP has been reported as a coactivator of estrogen receptor (ER) to induce the expression of estrogen-response elements [32–34]. The level of CBP has recently been found

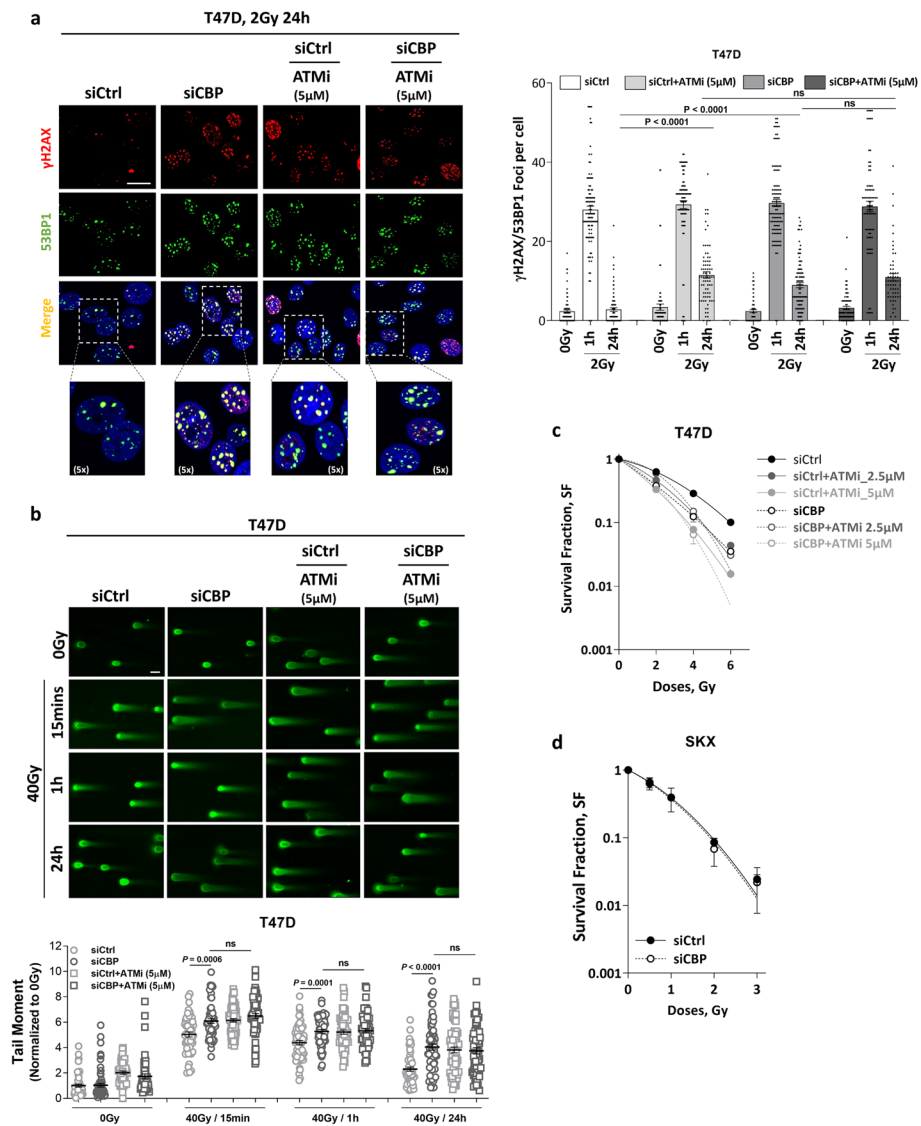


**Fig. 4** The effect of ATM inhibition on the repair of DNA double-strand breaks in CBP-depleted cells. **a** Left panel: Representative immunofluorescence images showing  $\gamma$ H2AX (red) and 53BP1 (green) foci at 24 h after 2 Gy ionizing radiation (IR) in T47D cells transfected with the indicated siRNAs and incubated with 5  $\mu$ M of ATM inhibitor (ATMi). Scale bar, 100  $\mu$ m. Right panel: Quantification of  $\gamma$ H2AX/53BP1 foci at 1 and 24 h post-IR from 100 cells. **b** Upper panel: Representative images of the neutral comet assay performed after the indicated times following 40 Gy IR. Scale bar, 50  $\mu$ m. Lower panel: Fold change of tail moment, calculated using OpenComet software, from 50 cells. **c** IR sensitivity of T47D cells transfected with negative control (siCtrl) or CBP (siCBP) siRNA for 48 h, followed by treatment with or without 2.5 or 5  $\mu$ M of ATMi for 2 h prior to irradiation. **d** Colony formation assay of ATM-deficient SKX cells transfected with the indicated siRNAs for 48 h before irradiation. Data are represented as mean  $\pm$  SEM,  $n = 3$ .  $P < 0.05$  is considered significant, Mann–Whitney  $U$  test. ns, not significant

to be positively correlated with ER status in breast cancer patients [14]. It is also known that the sensitivity of breast cancer patients to chemo- and radiotherapy is affected by the molecular characteristic of cancer cells, including ER status [35, 36]. Therefore, it is plausible to suggest a scenario whereby CBP regulates ATM and, consequently, DNA DSB through the ER. To test this hypothesis, we first treated ER-positive T47D cells

with 10 nM of the ER degrader, ICI 182780, for 4 h before irradiating them with 2 Gy and analyzing the colocalization of CBP with  $\gamma$ H2AX. Results revealed that the CBP- $\gamma$ H2AX PLA signal increased in T47D cells after 2 Gy in a similar manner, both with and without the addition of the ER degrader (Fig. 5a). Similarly, the CBP- $\gamma$ H2AX PLA signal was also increased in the ER-negative BT549 cells 5 min post-2 Gy (Fig. 5b), indicating an ER-independent recruitment of CBP to the DSB sites. The number of residual

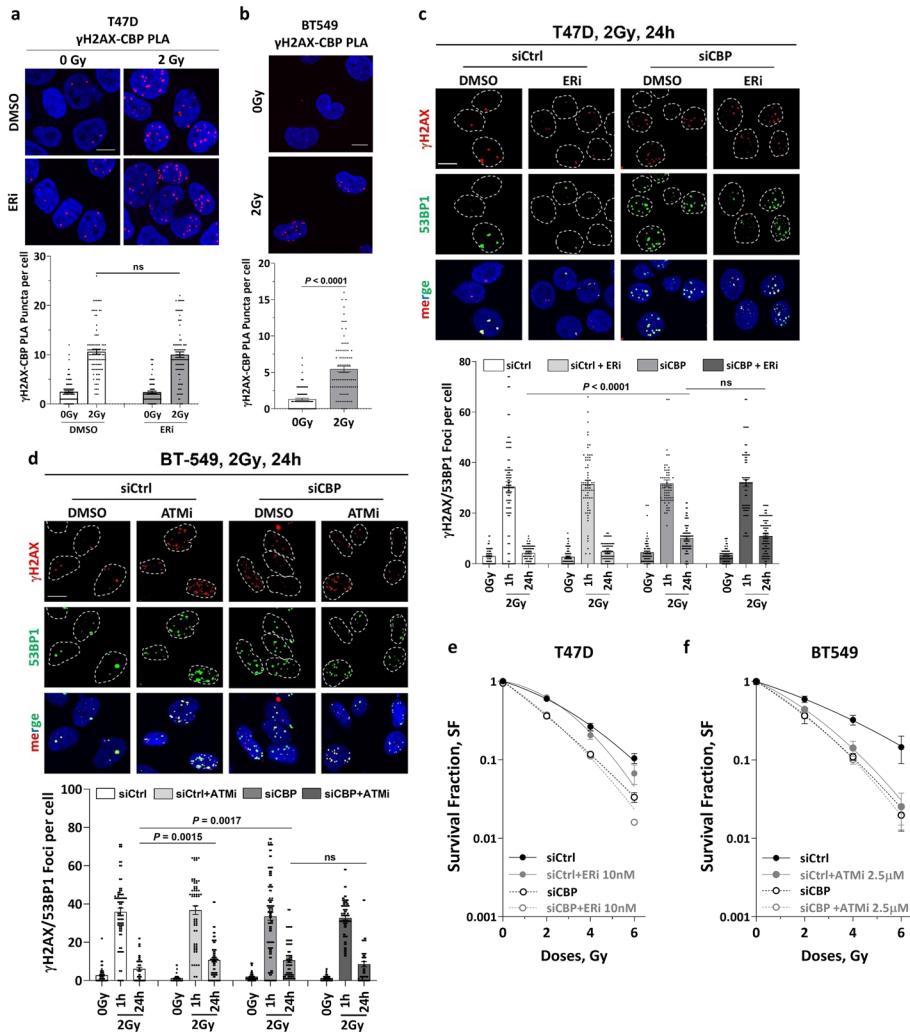


**Fig. 5** Role of CBP in DNA damage response is independent of ER. **a** Upper panel: T47D cells were treated with estrogen receptor inhibitor (ERI) 4 h before irradiation with 2 Gy. Proximity ligation assay (PLA) was performed to assess colocalization of  $\gamma$ H2AX and CBP at 5 min post-2 Gy ionizing radiation (IR). Scale bar, 100  $\mu$ m. Lower panel: Quantification of PLA signal for  $\gamma$ H2AX and CBP using ImageJ software from 100 cells. **b** Upper panel: PLA for  $\gamma$ H2AX and CBP colocalization after 5 min of 2 Gy IR in BT549 cells. Scale bar, 100  $\mu$ m. Lower panel: Quantification of PLA signals from 100 cells. **c, d** Upper panel: Representative images of immunofluorescence staining with anti- $\gamma$ H2AX (Red) and anti-53BP1 (green) antibodies in T47D cells treated with 10 nM of Eri ICI 182780 at 24 h post-IR (**c**) and BT549 cells treated with 5  $\mu$ M of ATM inhibitor (ATMi) at 24 h after 2 Gy IR (**d**). Scale bar, 100  $\mu$ m. Lower panel: Quantification data of colocalized  $\gamma$ H2AX and 53BP1 at 1 and 24 h of IR in T47D cells (**c**) and BT549 cells (**d**). **e, f** IR sensitivity of T47D cells (**e**) and BT549 cells (**f**) transfected with negative control (siCtrl) or CBP (siCBP) siRNA for 48 h, followed by treatment with and without ERI or ATMi before irradiation with the indicated doses. Data are represented as mean  $\pm$  SEM,  $n = 3$ .  $P < 0.05$  is considered significant, Mann-Whitney  $U$  test. ns, not significant

$\gamma$ H2AX/53BP1 foci at 24 h post-2 Gy was not changed in CBP-depleted T47D cells pre-treated with the ER degrader (Fig. 5c). Moreover, the number of  $\gamma$ H2AX/53BP1 foci in the ER-negative BT549 cells was significantly higher in CBP-depleted cells compared to non-depleted cells (Fig. 5d). Additionally, similar to what is reported for T47D cells in Fig. 4, no significant changes in the number of residual  $\gamma$ H2AX/53BP1 foci were found in CBP-depleted BT549 cells pre-treated with or without the ATMi (Fig. 5d). These data were recapitulated after damaging DNA with ETOP instead of IR (Additional file 1: Fig. S8). Further investigation demonstrated that ER inhibition slightly radiosensitized the T47D cells. More importantly, no further sensitization was detected in CBP-depleted T47D cells after ER degradation (Fig. 5e). CBP depletion enhanced radiosensitivity in BT549 cells. This radiosensitization effect was not further enhanced upon ATM inhibition (Fig. 5f), supporting the ATM-dependent function of CBP in ER-negative cells. Similar results were also reported in the lung cancer A549 cell line, where the ATM-dependent function of CBP in DSB repair was observed (Additional file 1: Fig. S9). Collectively, these results reveal that CBP regulates ATM activity in the response to DNA damage independently of ER.

#### **CBP interacts with ATM and regulates its recruitment at sites of DNA DSB**

Next, we sought to analyze the mechanism underlying CBP's role in ATM activation. Firstly, we tested whether CBP is required for ATM recruitment at DSB sites. To this end, CBP was depleted in T47D cells, and the recruitment of ATM at DSB sites was investigated by monitoring the ATM- $\gamma$ H2AX PLA signals after DNA damage. A significant reduction in the number of ATM- $\gamma$ H2AX PLA signals was observed 5 min post-2 Gy in CBP-depleted (Fig. 6a) and CBP KO clones (Fig. 6b).

On the other hand, inhibition of ATM activity by KU55933 under DOX treatment did not affect (i) the HAT activity of CBP, as indicated by the unchanged level of acetyl-p53 at lysine 382 (Fig. 6c) or (ii) the CBP- $\gamma$ H2AX co-existence, as measured by the PLA assay (Fig. 6d). These data suggest that CBP may function upstream of ATM in response to DNA damage. Previously, Jang et al. demonstrated that the CBP partner p300 is involved in acetylating and controlling the stability of NBS1 [37]. Since NBS1 mediates the recruitment of ATM to DNA damage sites [38], we investigated if CBP also modulates the stability of NBS1 in response to DNA damage. The time-course analysis of NBS1 expression after DOX treatment revealed no reduction in the level of NBS1 in CBP-depleted cells compared to their wild-type counterparts (Additional file 1: Fig. S10a). Furthermore, the recruitment of NBS1 to DNA damage sites remained unaffected by CBP loss (Additional file 1: Fig. S10b, c), excluding the involvement of NBS1 in the CBP-ATM axis.

Based on the apparent link between CBP and ATM, we speculated that they bind directly to each other. In line with this assumption, co-immunoprecipitation analysis revealed that CBP forms a complex with ATM independent of DNA. However, their interaction was further augmented upon DNA damage induced by DOX in T47D cells (Fig. 7a, b). Reciprocal immunoprecipitation further validated the CBP-ATM interaction (Additional file 1: Fig. S11a). Similar results were observed in MCF7 cells, reinforcing the notion of a direct association between CBP and ATM, which is strengthened upon DNA damage (Additional file 1: Fig. S11b). Interestingly, ATM phosphorylation

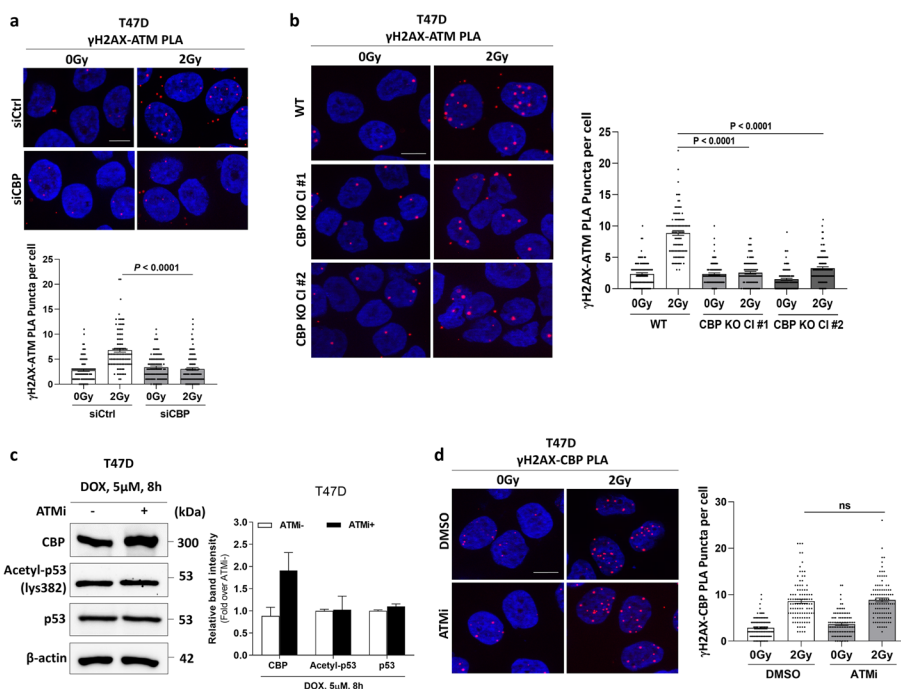


**Fig. 6** CBP is required for recruitment and activation of ATM at sites of DNA double-strand breaks. **a** Upper panel: Proximity ligation assay (PLA) analysis for  $\gamma$ H2AX and ATM colocalization after 5 min of 2 Gy IR in T47D cells transfected with the indicated siRNAs. Scale bar, 100  $\mu$ m. Lower panel: Quantification of PLA signals from 100 cells. **b** Left panel: T47D wild-type (WT) and CBP knockout (KO) clones 1(CI #1) and 2 (CI #2) irradiated with 2 Gy. PLA analysis was performed 5 min post-irradiation using anti- $\gamma$ H2AX and anti-ATM antibodies. Scale bar, 100  $\mu$ m. Right panel: Graph depicting PLA signal quantification from 100 cells. **c** Left panel: Representative immunoblot images for CBP, acetyl-p53 and p53 in T47D cells after incubation with ATM inhibitor (ATMi) for 2 h followed by Doxorubicin (DOX) exposure for 8 h. Right panel: Quantification of the band intensities for the indicated proteins, normalized to  $\beta$ -actin. **d** Left panel: T47D cells treated with ATMi 2 h before irradiation. PLA was performed using anti- $\gamma$ H2AX and anti-CBP antibodies. Scale bar, 100  $\mu$ m. Right panel: Quantification of PLA signals using ImageJ software from 100 cells. Data are represented as mean  $\pm$  SEM,  $n = 3$ .  $P < 0.05$  is considered significant, Mann-Whitney  $U$  test. ns, not significant

was increased in the CBP immunoprecipitated samples after DNA damage (Fig. 7b). Using a PLA assay, we recapitulated the direct association between the two proteins after IR by demonstrating higher colocalization between CBP and ATM at 5 min, which then decreased after 30 min post-2 Gy (Fig. 7c), indicating the involvement of CBP in the early events of DDR. Supporting the data in Fig. 1d that CBP mainly contributes to the response to DSBs, CBP-ATM colocalization was enhanced after treatment with the DSB inducer ETOP but was clearly lower after treatment with the DNA cross-linker CIS compared to IR exposure (Fig. 7c; Additional file 1: Fig. S11c). Again, the enhanced ATM-CBP colocalization by ETOP or IR was independent of ER (Additional file 1: Fig. S11c-e). These data collectively reveal that CBP regulates DDR through interaction with ATM to facilitate its recruitment and activation, mainly upon DSBs induction.

Interestingly, PLA signals for ATM-CBP and, to a lesser extent, for ATM- $\gamma$ H2AX were also observed outside of the DAPI-stained regions. These extra-DAPI PLA signals can be attributed to the extra-chromatid role of ATM in DDR, including its cytoplasmic interactions and responses to oxidative stress [39–41]. In the nucleus, ATM functions on chromatin by phosphorylating H2AX and chromatin-related substrates, as well

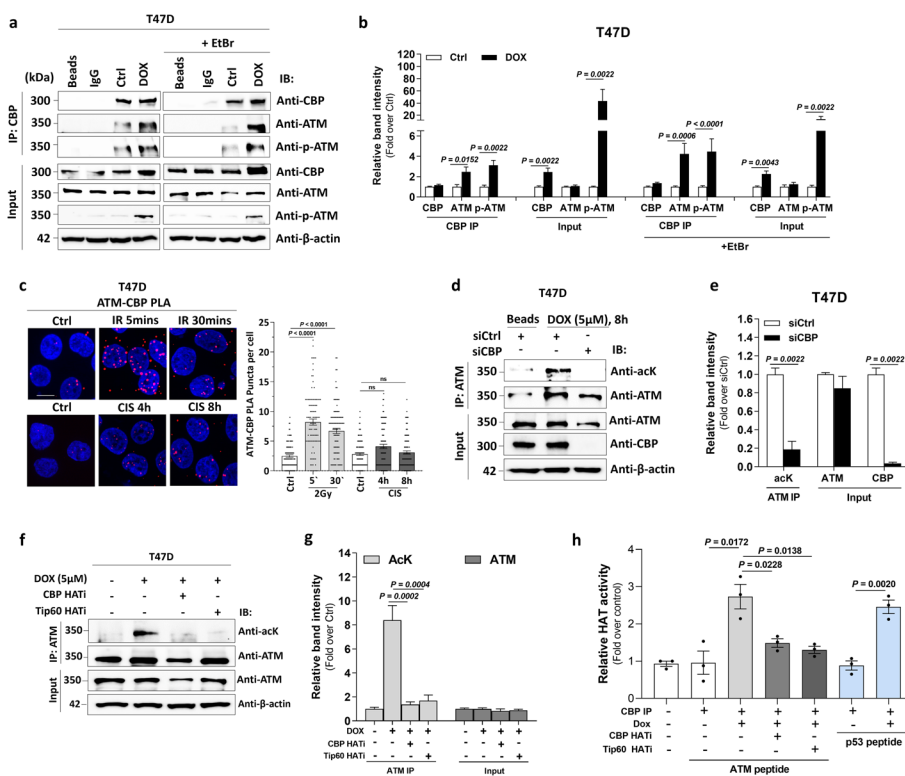


**Fig. 7** CBP binds to and acetylates ATM in response to DNA damage. **a** Immunoprecipitation (IP) of CBP from T47D cells treated with Doxorubicin (DOX) for 8 h. The cell extracts were pretreated with and without ethidium bromide (EtBr). Immunocomplexes were analyzed by immunoblotting using the indicated antibodies. **b** Band quantification of CBP, ATM, and p-ATM levels in both immunoprecipitated and input samples. **c** Left panel: Proximity ligation assay (PLA) for CBP and ATM colocalization (red) in T47D cells after ionizing radiation (IR) or after incubation with 5  $\mu$ M Cisplatin (CIS). DAPI staining (blue) shows the nucleus. Scale bar, 100  $\mu$ m. Right panel: Bar graphs representing the quantification of PLA signals from 100 cells. **d** T47D cells transfected with the indicated siRNAs for 48 h were incubated with DOX. Cell lysates were subjected to immunoprecipitation using ATM antibody. The acetylation level was determined by immunoblotting using anti-acetyl lysine (anti-ack) antibody. **e** Band intensities for acetyl lysine in ATM-immunoprecipitated samples, and for ATM and CBP in input samples, normalized to  $\beta$ -actin. **f** T47D cells were incubated with CBP HAT or Tip60 HAT inhibitors, followed by DOX treatment. After 8 h, the cells were collected, and immunoprecipitation was performed using anti-ATM antibody followed by immunoblotting with anti-acetyl lysine (anti-ack) antibody. **g** Densitometric quantification of acetyl-ATM levels in T47D cells treated with the indicated inhibitors and DOX. **h** CBP was immunopurified from T47D cells treated with 8  $\mu$ M of CBP HAT inhibitor or 25  $\mu$ M of Tip60 HAT inhibitor, followed by DOX treatment. ATM acetylation activity was assessed by measuring the release of free CoA via absorbance at 570 nm in the presence of tetrazolium dye. Data are represented as mean  $\pm$  SEM,  $n = 3$ .  $P < 0.05$  is considered significant, Mann–Whitney  $U$  test

as extra-chromatin, regulating the cell cycle through phosphorylation of Chk1/2 and related genes.

### CBP mediates ATM activity through acetylation

ATM has been reported to undergo rapid acetylation in response to DSBs, which is demonstrated to be critical for the activation of its kinase activity [8]. Since CBP retains HAT activity, it was rational to speculate that CBP may be involved in the acetylation of ATM upon DNA damage. Therefore, we set out to examine the acetylation of ATM in CBP-downregulated T47D cells following DOX treatment. The acetylation level of ATM was measured using a previously characterized acetyl lysine-specific antibody [42]. ATM was

immunoprecipitated from CBP-depleted T47D cell lysates, followed by immunoblotting with a pan-acetyl-lysine antibody. Notably, CBP depletion led to a reduction in the acetyl-ATM levels upon DNA damage induced by DOX in T47D cells (Fig. 7d, e). To strengthen the hypothesis that CBP's HAT activity is involved in ATM acetylation, we pre-treated the cells with 8  $\mu$ M of the CBP HAT inhibitor C646. This treatment resulted in a notable reduction in ATM acetylation levels, an effect comparable to that seen with the Tip60 HAT inhibitor NU9056 (Fig. 7f, g). Additionally, we measured the HAT activity of CBP derived from DOX-treated T47D cells using an ATM peptide corresponding to amino acid sites 3007 to 3024, which contains the only site previously shown to be acetylated in ATM, namely lysin 3016 [43]. As shown in Fig. 7h, the immunoprecipitated CBP potently acetylates ATM peptide containing lysine 3016 following exposure to DOX as efficiently as the positive control p53 peptide. Pre-treating the cells with CBP HAT inhibitor prevented the DOX-induced acetylation of the ATM peptide. A similar effect was observed when the cells were pre-treated with the Tip60 HAT inhibitor.

In line with the idea of ATM acetylation by CBP, the number of ATM- $\gamma$ H2AX PLA signal at 5 min post-2 Gy was significantly decreased upon inhibition of CBP HAT activity in T47D cells using the C646 inhibitor (Additional file 1: Fig. S12a). A similar effect was observed upon inhibition of Tip60 HAT activity. Furthermore, the phosphorylation of ATM and its downstream target Chk2 were reduced after inhibition of CBP HAT activity (Additional file 1: Fig. S12b). Consequently, depletion or inhibition of CBP enhanced the sensitivity of T47D cells to DOX (Additional file 1: Fig. S12c, d). To ensure that CBP and Tip60 are not compensating for each other in the regulation of ATM acetylation and activation, we measured ATM acetylation and phosphorylation under conditions where the HAT activity of CBP and Tip60 was inhibited both individually and in combination (Additional file 1: Fig. S12e, f). Our results demonstrate that inhibition of either CBP or Tip60 individually led to a reduction in ATM acetylation and downstream phosphorylation of ATM, Chk2, and p53. Notably, when both acetylases were inhibited simultaneously, the reduction in protein activation was slightly pronounced, indicating that CBP and Tip60 do not completely compensate for each other in regulating ATM acetylation and activation.

To further validate the critical role of CBP HAT activity in DSBs repair, we transfected CBP KO T47D cells with a plasmid expressing GFP-CBP HAT domain. Complementation with the HAT domain rescued DNA repair in CBP KO cells as evidenced by a significantly lower number of  $\gamma$ H2AX foci in GFP-positive cells compared to GFP-negative cells (Fig. 8a). Of note, the CBP bromodomain, but not the CH3-domain could also rescue repair efficiency in CBP KO cells (Fig. 8a), indicating a role for the bromodomain of CBP in DSB repair. These results were further reflected in the ability of the wild-type, but not the mutant, HAT domain of CBP to rescue DNA DSB repair efficiency in CBP KO cells (Fig. 8b). Taken together, these results suggest that CBP contributes to ATM acetylation and activation in response to DSBs.

## Discussion

The findings here show that CBP plays a significant role in the cellular response to DNA damage through the acetylation and activation of ATM upon induction of DNA DSBs.

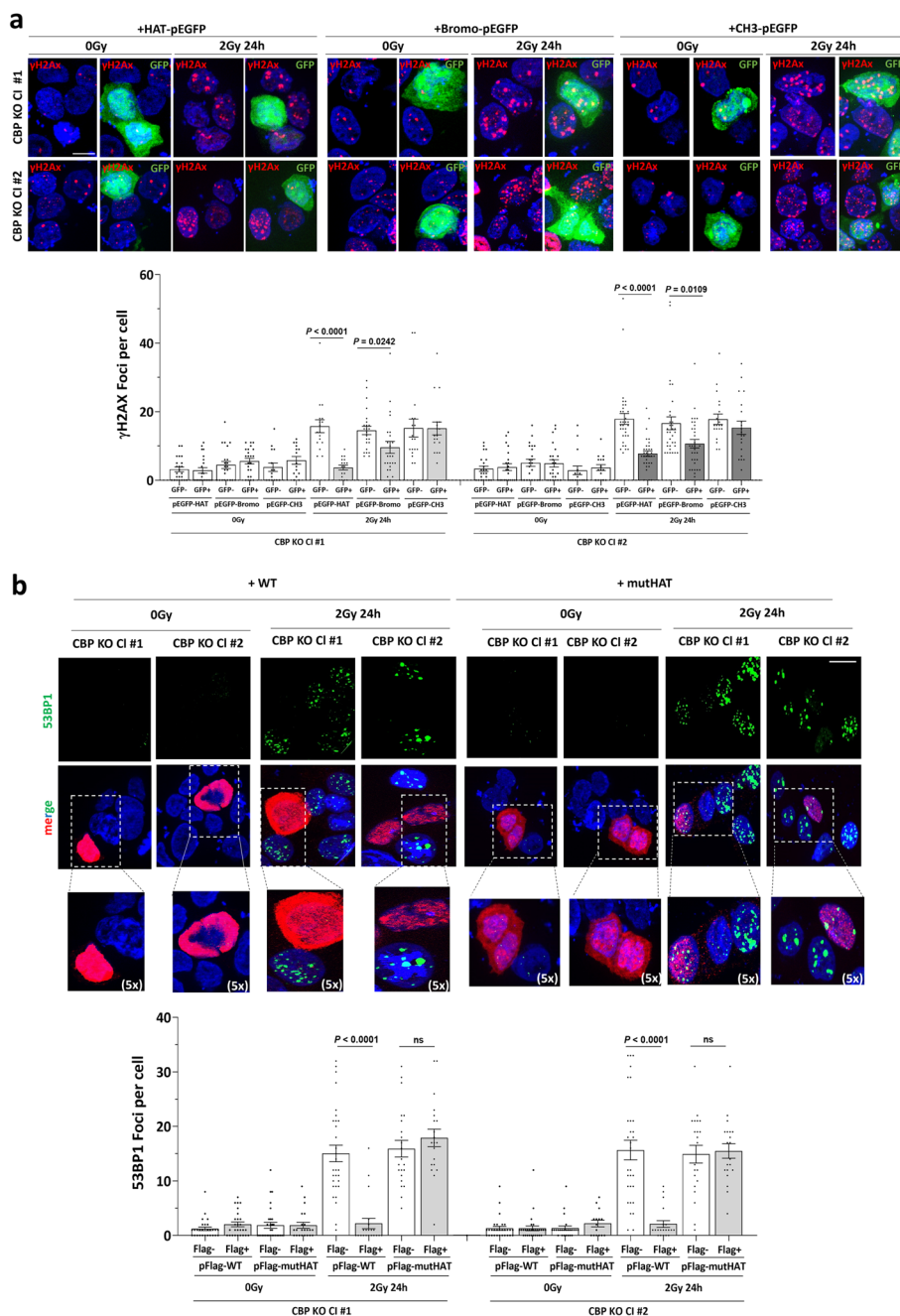


**Fig. 8** Complementation with CBP restores DNA damage repair in irradiated-CBP knockout T47D cells. **a**, **b** Upper panel: T47D CBP knockout (KO) cells were transfected with the indicated plasmids and irradiated with 2 Gy. Immunofluorescence analysis was performed for  $\gamma$ H2AX (red) (**a**), 53BP1 (green), and Flag (red) (**b**) after 24 h of ionizing radiation (IR). Scale bar, 100  $\mu$ m. Lower panel: Quantification of  $\gamma$ H2AX foci (red) per cell was done in green fluorescence protein (GFP)-positive cells versus GFP-negative cells for **a**. Quantification of 53BP1 (green) foci per cell was done in Flag-positive cells (red) versus Flag-negative cells for **b**. Data are represented as mean  $\pm$  SEM from 20 cells,  $n = 3$ .  $P < 0.05$  is considered significant, Mann–Whitney  $U$  test

The level of CBP was found to be increased in cells undergoing DNA damage, due to enhanced stability. This is in line with the previously reported CBP stabilization after DNA damage induction through inhibiting its proteasomal degradation by iASPP [44]. As a consequence of its increased stability, the CBP HAT activity was also stimulated, as

evidenced by the elevated level of p53 acetylation at lysine 382 following DNA damage. While several acetyltransferases, including p300, pCAF, Tip60, MOF, and MOZ, contribute to the acetylation of p53 [45], CBP/p300 is the most extensively studied acetyltransferase responsible for acetylating p53 in response to DNA damage. This was further supported by our *in vitro* data showing p53 acetylation by CBP under DOX treatment. Moreover, our findings revealed that downregulation of CBP significantly reduced acetyl-p53 levels, further supporting CBP's role in p53 acetylation.

In addition, the recruitment of CBP to DNA damage lesions was observed at early time points following DNA damage induced by IR or ETOP, however to a lesser extent after MMC or CIS, indicating CBP's involvement in the response to DNA DSBs. Previous data have reported that ATM is acetylated by the HAT Tip60 at lysine 3016 [43]. This acetylation occurs concurrently with H2AX phosphorylation and ATM autophosphorylation, making ATM acetylation at this site crucial for ATM's kinase activity under DNA damage [43]. Our findings demonstrate that ATM is a substrate of CBP-dependent acetylation in response to DNA DSBs. After DOX exposure, CBP likely acetylates ATM at lysine 3016 *in vitro*. In support of this, a marked reduction in the level of ATM acetylation was observed under DOX-induced DNA damage following CBP depletion or inhibition of its HAT activity. The lysine 3016 residue is located in the FATC domain of ATM, which is reported to be mutated or deleted in patients with ataxia telangiectasia (AT) and B cell chronic lymphatic leukemia [46, 47]. Based on our data here, the ATM-deficiency phenotype in these patients could be attributed to the absence of ATM acetylation by CBP.

The HAT Tip60 binds to and acetylates ATM at the FATC domain in response to DNA damage. Since we have demonstrated that CBP mainly responds to DSB induction and to a lesser extent to other forms of DNA damage, such as DNA crosslinks, we propose that both CBP and Tip60 play critical roles in ATM acetylation. Their activation likely occurs through a cooperative mechanism within a shared complex, suggesting that they do not fully compensate for each other in regulating ATM acetylation and activation. This is supported by the observation that inhibiting either CBP or Tip60 individually reduces ATM acetylation, while the combined inhibition of both acetylases results in a slightly greater reduction in ATM activation and its downstream signaling proteins.

We propose that the initial step in the activation of ATM-dependent DDR is the stimulation of CBP HAT activity. Current data indicate that CBP acts upstream of ATM, as supported by (i) impaired phosphorylation of ATM and its downstream target Chk2 following DSB induction after CBP depletion or inhibition and (ii) the failure of the ATM kinase inhibitor KU55933 to prevent either the recruitment of CBP or the activation of CBP HAT domain upon DNA damage. The involvement of HAT activity in the described CBP role in DNA DSB repair was further confirmed by the rescue effect of re-introducing the wild-type, but not the mutated, CBP HAT domain into CBP KO cells.

Although our findings suggest an upstream role for CBP in modulating ATM activation, a recent study has highlighted that ATM-mediated CBP phosphorylation catalyzes the lactylation of MRE11, rather than its acetylation. MRE11 lactylation is essential for DNA end resection and, consequently, facilitates HR repair. This implies that ATM-mediated phosphorylation of CBP may regulate its function as a lactate transferase, without affecting its acetyltransferase activity, thereby influencing DNA DSB repair

processes [48]. Supporting this, our findings indicate that inhibition of ATM activity does not affect CBP-mediated acetylation of p53. Collectively, there may be an overlap in the metabolic pathways regulated by CBP. The distinct roles of CBP as a lactyltransferase and acetyltransferase may reflect the complexity of its function in the DDR. Future research is necessary to clarify these mechanisms and further delineate the role of CBP in regulating DNA repair processes in different contexts.

In addition to the HAT domain, CBP contains other highly conserved domains, including CH3 domain, which mediates interactions with various cellular transcription factors, and the bromodomain, which recognizes and binds acetylated histone tails. Bromodomain-containing proteins are key regulators of the DDR, interpreting acetylation marks within chromatin to activate DDR pathways and chromatin-related activities essential for genome-epigenome maintenance. As a result, DDR pathways involving bromodomain proteins play a critical role in safeguarding genome integrity and maintaining normal cellular functions [49]. This may explain the observed restorative effect of the CBP bromodomain under DNA damage conditions. Supporting previous findings, the CBP bromodomain plays a critical role in preparing nucleosomes around DSBs, facilitating CBP recruitment and localization to DNA damage sites, thereby initiating DNA repair processes [27]. Importantly, inhibition of the CBP bromodomain has been shown to significantly impair DNA repair at damage sites [50]. These findings emphasize the importance of the CBP bromodomain in maintaining efficient DNA repair, likely independent of its role in regulating ATM activity.

The exact mechanism of CBP recruitment to DNA damage sites still needs further investigation. Manickavinayam et al. showed that CBP acetylates E2F1 via its HAT domain, facilitating E2F1 recruitment to DNA damage sites and enhancing subsequent CBP recruitment through its bromodomain [27]. However, previous studies reported that the accumulation of E2F1 at DNA damage sites is dependent on ATM kinase activity [51, 52]. Notably, knock-in mutations that prevent E2F1 acetylation resulted in reduced ATM phosphorylation, though a residual level of active ATM remained. Based on these findings and our own data, we hypothesize that E2F1 acetylation by CBP may play a role upstream of ATM activation and recruitment [27]. Upon enhancement of its kinase activity, ATM is recruited at sites of DNA damage, where it undergoes autophosphorylation at serine 1981, causing its monomerization and subsequent activation and stabilization at the DNA damage sites [53, 54]. In contrast to a previous investigation that revealed a role for ATM upstream of CBP paralog p300 in stabilizing NBS1 [37], our study proposes an upstream role of CBP in ATM activation and further suggests that NBS1 is not implicated in CBP-mediated regulation of the ATM-dependent DDR cascade.

Given the fundamental role of ATM in maintaining genomic stability, its deficiency leads to defects in repairing DNA DSBs, resulting in enhanced radiosensitivity [55]. Consistent with CBP's role in regulating ATM activity, depletion or inhibition of CBP impaired DNA DSB repair, as demonstrated by the increased accumulation of  $\gamma$ H2AX and 53BP1 foci and the increase in tail moment at 24 h post-IR, as well as after the removal of DOX. The contribution of CBP to efficient DNA repair was further reflected by the increased sensitivity of CBP-depleted or knockout cells to DOX or IR, which is in line with previous studies conducted in

other cancer types like leukemia, lung, and colon cancers [19–21]. We provide several pieces of evidence supporting that CBP's role in regulating DDR is ATM-dependent, as follows: (i) Inhibiting ATM activity in CBP-depleted cells neither further reduce the DNA repair efficiency after induction of DSBs by IR or ETOP nor altered the radiosensitivity of breast cancer cells. (ii) Depletion of CBP did not further inhibit DSB repair or increase radiosensitivity in the previously reported ATM-deficient SKX cells. Our findings suggest that CBP plays a role in the initial recognition of DNA DSBs by unleashing the full activity of ATM. While ATM expression was not significantly affected in CBP knockdown models or upon CBP HAT inhibition, it was differently downregulated in the two CBP KO clones. This reduction may be attributed to the absence of CBP, potentially causing extensive chromatin remodeling and leading to a more compact chromatin structure that hinders the transcription of multiple genes, including ATM. In contrast, the residual CBP present in knockdown cells might be sufficient to maintain chromatin relaxation, thereby preserving ATM protein levels. However, the observed differences in ATM expression did not affect CBP's role in mediating ATM activation, as evidenced by (i) consistent impairments in phosphorylation of ATM across both CBP-depleted and CBP KO cells, irrespective of ATM expression levels; (ii) both CBP KO clone, despite exhibiting differing levels of ATM expression, displayed similar severe impairments in p-ATM signaling, downstream target activation, DSB repair efficiency, and sensitivity to DOX treatment.

CBP/p300 has been previously associated with the DNA repair machinery. On the one hand, CBP induces histone acetylation, enhancing the transcriptional activation of HR repair genes [25]. On the other hand, CBP/p300 associates with SWI/SNF-mediated chromatin relaxation [23, 56, 57], leading to increased H2AX phosphorylation [56]. However, no change in ATM expression, activation, or ATM-mediated DDR was observed. Interestingly, another study revealed that ATM phosphorylates the catalytic subunit of SWI/SNF to fully activate DDR after inducing DSBs [57], suggesting that ATM functions upstream of the SWI/SNF complex in the DDR. Together, these findings indicate that the roles of CBP in DNA repair, as previously described, occur after the recognition of DSBs, primarily by ATM [56, 57]. Based on the current study and the previously reported role of CBP in DDR, it is tempting to assume that the recruitment of CBP following DNA damage leads to (i) ATM acetylation, which facilitates the focal recruitment of downstream signaling proteins, and (ii) histone acetylation to enhance chromatin accessibility for DNA repair proteins.

Previous data have revealed crosstalk between the DDR machinery and the ER signaling pathway. In particular, ER $\alpha$  negatively regulates the expression of ATM through activating microRNA 18a and 106a, leading to the accumulation of DNA damage [58]. Since CBP co-activates diverse transcription factors, including the ER [59], we tested the involvement of ER in CBP's role in ATM-dependent DDR. Several controls were conducted to exclude this possibility, as follows: (i) CBP depletion in ER-positive T47D cells showed similar levels of DNA repair deficiency and radiosensitization effects, both with or without chemical degradation of ER; (ii) ER-negative BT549 cells showed an increased number of residual  $\gamma$ H2AX and 53BP1 foci at 24 h post-IR along with enhanced radiosensitivity upon CBP depletion; (iii)

the co-localization of CBP with either ATM or  $\gamma$ H2AX after IR or ETOP was similarly increased in both T47D (ER-positive) and BT549 (ER-negative) cells as well as in T47D cells treated with or without the ER degrader; and (iii) a similar effect was observed upon CBP depletion in lung cancer A549 cells.

**Conclusions**

In conclusion, we propose a previously unreported role for CBP in the early events of the DDR pathway leading to DNA DSB repair (Fig. 9). Following the induction of DNA DSBs, CBP becomes stabilized and directly binds to ATM. Through its HAT activity, CBP acetylates ATM, a crucial step for ATM autophosphorylation and full activation, which triggers the subsequent DDR cascade and DSB repair. Future investigations into the translational significance of CBP-mediated ATM acetylation are warranted, as these may lead to the identification of new therapeutic strategies to modulate the cellular response to DNA-damaging agents in cancer.

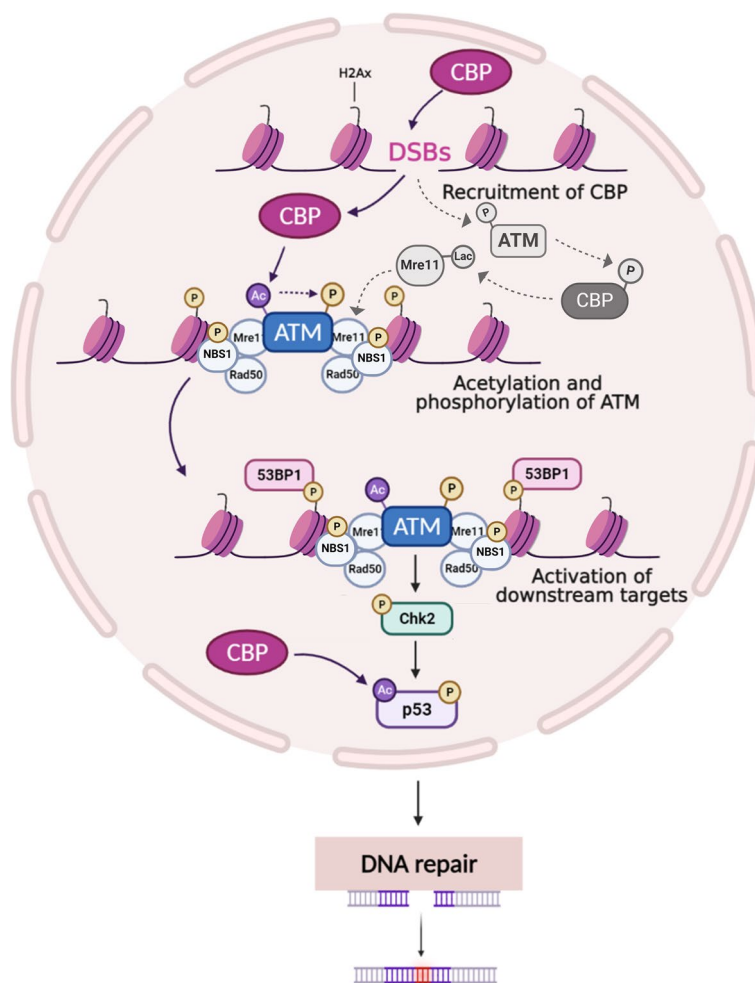


**Fig. 9** Proposed model of the involvement of CBP in DNA damage response pathway [48]

## Methods

### Antibodies

The following antibodies were used: CBP (Cell signaling Technology, USA, Cat # 7389),  $\gamma$ H2AX Ser139 (Cell signaling Technology, USA, Cat # 9718), H2AX (Cell signaling Technology, USA, Cat # 2595), p-ATM Ser1981 (Cell signaling Technology, USA, Cat # 5883), ATM (Cell signaling Technology, USA, Cat # 2873), p-Chk2 Thr68 (Cell signaling Technology, USA, Cat # 2197), Chk2 (BD biosciences, USA, Cat # 611,570), p-ATR Thr1989 (Cell signaling Technology, USA, Cat # 30,632), ATR (Cell signaling Technology, USA, Cat # 2790), p-Chk1 Ser348 (Cell signaling Technology, USA, Cat # 2348), Chk1 (Cell signaling Technology, USA, Cat # 2360), p-p53 Ser15 (Cell signaling Technology, USA, Cat # 9286), Acetyl-p53 Lys382 (Cell signaling Technology, USA, Cat # 2525), p53 (Santa Cruz Biotechnology, USA, Cat # S126), p21 (Cell signaling Technology, USA, Cat # 2947), Acetyl-lysine (Cell signaling Technology, USA, Cat # 9441), NBS1 (Cell signaling Technology, USA, Cat # 14,956),  $\beta$ -actin (Sigma-Aldrich, Germany, Cat # A5441), p-ATM (Invitrogen, USA, Cat # MA1-2020), ATM (Invitrogen, USA, Cat # MA1-23,152, 1:200), p-H2AX S139 (Millipore, USA, Cat # 23,464), 53BP1 (Novus, USA, Cat # NB100-304), Flag (Sigma-Aldrich, Germany, Cat # F1804), CBP (Santa Cruz Biotechnology, USA, Cat# sc-7300) and p-ATM (Abcam, UK, Cat# ab81292).

### Cell culture, treatment, and irradiation

MCF7 (RRID:CVCL\_0031), T47D (RRID:CVCL\_0553), and BT-549 (RRID:CVCL\_1092) breast cancer cell lines and A549 (RRID:CVCL\_0023) lung cancer cell line (ATCC, VA, USA) were obtained from the Radiobiology and Experimental Radio-Oncology lab, University Medical Center, Hamburg University, Hamburg, Germany. The cells were cultured in RPMI (Sigma Aldrich, Germany) supplemented with 10% fetal bovine serum and 1% penicillin/streptomycin (Sigma Aldrich, Germany) at 37 °C in 5% CO<sub>2</sub>. ATM-deficient cells (SKX) were established from biopsy obtained from head and neck cancer patient at the University of Hamburg in 1991 [60]. SKX cells were grown in DMEM supplemented with 10% fetal bovine serum and 1% penicillin/streptomycin. All cell lines used in this study were routinely authenticated by short tandem repeat (STR) DNA profiling using Powerplex 16HS System (Cell line services GmbH, Eppelheim, Germany). All experiments were performed with mycoplasma-free cells.

Cell irradiation was done at room temperature with X-rays operated at 200 kVp and 15 mA with additional 0.5-mm Cu filter at a dose rate of 0.8 Gy/min. To induce DNA damage, cells were treated with 5  $\mu$ M of Doxorubicin (Sigma-Aldrich, Cat # D1515), Etoposide (Sigma-Aldrich, Cat # E1383), Cisplatin (Sigma-Aldrich, Cat # C2210000), and Mitomycin C (Sigma-Aldrich, Cat # M4287) for 8 h. To inhibit kinase activity of ATM, 2.5 and 5  $\mu$ M of KU55933 (Selleckchem, Cat # 118,500) was used. To inhibit histone acetyltransferase activity of CBP and Tip60, 8  $\mu$ M of C646 (Sigma Aldrich, Cat # SML0002) and 25  $\mu$ M of NU9056 (abcam, Cat # ab255734) were used, respectively. Estrogen receptor antagonist ICI 182780 (abcam, Cat # ab120131) was used at 10 nM concentration to degrade estrogen receptor.

### CRISPR/CAS9-mediated CBP knockout cells

T47D cells were transfected with pLentiCRISPR-v2 plasmids encoding two CREBBP gRNAs and caspase 9 (GeneScript, Cat # SC1805). The transfected cells were selected with puromycin antibiotic (Sigma-Aldrich, Cat # P7255) and single colonies were isolated and tested by immunoblotting. *CREBBP* guide RNA sequences were used as follows:

Human *CREBBP* guide RNA 1: 5'-AGCGGCTCTAGTATCAACCC-3'

Human *CREBBP* guide RNA 2: 5'-GAATCACATGACGCATTGTC-3'

### siRNA, plasmids, and transfection

To transiently knockdown the expression of CBP, cells were transfected for 48 h with 50 nM of siRNA for CBP (Dharmacon, Cat # L-003477-00-0005) using lipofectamine RNAiMAX reagent (Thermo Fisher scientific, Cat # 13,778) following the manufacturer's recommendations. Non-targeting siRNA (Dharmacon, Cat # D-001820-01-05) was used as negative control.

In complementation studies, T47D CBP knockout cells were transfected for 24 h with different plasmid constructs using turbofect transfection reagent (Thermo Scientific, Cat # R0531). Expression plasmids for different CBP domains including HAT, Bromo, and CH3 were generated by subcloning the coding sequences from CBP-HAT-Sp65 (Addgene, Cat # 21,088), CBP-Bromo-SP65 (Addgene, Cat # 21,089), and CBP-CH3-SP65 (Addgene, Cat # 21,092) plasmids into pEGFP-N1 plasmid (Invitrogen, USA) to express eGFP-labeled CBP domains in cells. Expression vectors for wild-type CBP (pcDNA3β-FLAG-CBP-HA, Cat # 32,908) and mutated HAT CBP (pcDNA3β-FLAG-CBP-LD-HA, Cat # 32,906) fused to FLAG tag at N-terminus were purchased from Addgene.

### Cycloheximide chase assay

The stability of CBP protein has been measured under DNA damage by cycloheximide chase assay. The kinetics of protein biosynthesis inhibition by cycloheximide (Cell signaling technology, Cat # 2112) treatment was done with and without induction of DNA damage by 5 μM of DOX or by irradiation with 10 Gy. The cells were collected and lysed at different time points (4, 8, 12, and 24 h). The stability of CBP was monitored by measuring its level using immunoblotting.

### Immunoprecipitation

The cells were harvested in 1X PBS after treatment and resuspended in triton lysis buffer (25 mM Tris-HCl H 7.4, 150 mM NaCl, 1% Tritonx-100, 1 mM EDTA) containing protease/phosphatase inhibitors cocktail (Sigma-Aldrich, Cat # MSSAFE). For acetylation measurement, sodium butyrate (Sigma-Aldrich, Cat # B5887) was added to the triton lysis buffer. The protein A/G Sepharose (Abcam, Cat # ab193262) beads were conjugated with IgG or CBP or ATM primary antibody and incubated on ice for 2 h. After conjugation, an equal amount of cell lysates (some amounts were saved to load as input) was added to the beads-antibody complex and incubated at 4 °C for 2 h with gentle shaking. After 2 h, immunocomplexes were eluted by heating at 95 °C

with 1X laemmli buffer. The immunoprecipitated and input samples were loaded in SDS-PAGE gels.

#### SDS PAGE and immunoblotting

Analysis of the protein level was performed as described previously [61]. The cell lysates were harvested using lysis buffer (20% SDS, glycerol, 1 M Tris (pH 6.8)) containing protease/phosphatase inhibitors cocktail (Sigma-Aldrich, Cat # MSSAFE). An equal amount of proteins (10 or 20  $\mu$ g) were separated in 8 or 12% SDS-PAGE or tris-acetate gradient gel (3–8%) as previously described [62], and then transferred into nitrocellulose membrane (Bio-rad, Cat # 1,620,115), followed by immunoblotting with specific primary antibody overnight at 4 °C. In the next day, the membrane was incubated with secondary anti-rabbit or anti-mouse IgG, HRP-conjugated antibody (Cell Signaling Technology, Cat #7076 and #7074, 1:2000) for 1 h at room temperature. The membrane was subjected to ECL (Enhanced Chemiluminescence) detection (Biorad, Cat # 1705061) and developed using ChemiDoc™ imaging system (Biorad, USA).

#### HAT assay

CBP was immunoprecipitated from T47D cells and eluted from the beads using a buffer containing 0.2 M glycine pH 2.5 and subsequently neutralized with 1 M Tris-base pH 10.8. The HAT activity of CBP was measured using HAT activity colorimetric assay kit (Sigma-Aldrich, Cat # EPI001) following the manufacturer's protocol. Eluted CBP was incubated in HAT assay buffer containing 100  $\mu$ M of acetyl-CoA (Sigma-Aldrich, Cat # A2056) and either ATM peptide (ERVLMRLQEKLKGVVEGT) or p53 peptide (SHLK-SKKGQSTSRHKLMFK) (GeneScript, USA) at 37 °C. Colorimetric change representing the release of CoA was measured by plate reader Varioskan™ Flash (Thermo Fisher scientific, USA) at 570 nm.

#### Quantitative real-time PCR

The mRNA levels were analyzed by quantitative real time—polymerase chain reaction (RT-PCR) [63]. RNA was isolated using total RNA extraction kit (Norgen Biotek, Cat # 17200) followed by synthesizing the complementary DNA by TruScript Reverse Transcriptase Kit (Norgen Biotek, Cat # 54420) following the manufacturer's instructions. cDNA samples were quantified using Nanodrop 2000 (Thermo Fisher Scientific, USA). The RT-PCR was performed by Rotor-Gene Q (Qiagen, USA) using GoTaq qPCR master mix (Promega, Cat # A6001) according to the manufacturer's instructions. The data was quantified using  $2^{-\Delta\Delta C_t}$  method after normalization to *GAPDH* level. The *CREBBP* primer sequences (Forward: 5'-GAATCAGCTCTTCCGACTTC-3', Reverse: 5'-TGC CAGCCTTTTCCCTTACA-3'). The *GAPDH* primer sequences (Forward: 5'-CCTGCA CCACCAACTGCTTA-3', Reverse: 5'-GGCCATCCACAGTCTTCTGAG-3').

#### Immunofluorescence

Immunofluorescence analysis of  $\gamma$ H2AX, 53BP1, NBS1, and p-ATM was performed as previously described [64]. In brief, cells grown on coverslips were fixed with 4% formaldehyde for 10 min and permeabilized with 0.2% Triton X-100/PBS for 15 min. The coverslips were blocked with 3% BSA/PBS for 1 h and incubated for 1 h at room

temperature with primary antibodies. The anti-rabbit Alexa Fluor 488 and anti-mouse Alexa Fluor 594-conjugated secondary antibodies (Cell signaling technology, Cat #4412 and #8890, 1:1000) were added to the coverslips for 1 h at room temperature in the dark. The nuclei were stained with 4'-6-diamidino-2-phenylindole (DAPI) (Sigma-Aldrich, Cat # 28,718-90-3). The coverslips were mounted on microscopic slides using Vectashield mounting medium (Vector Laboratories, Cat # H-1000) and were visualized by AxioObserver.Z1 fluorescence microscope (Zeiss, Germany) using 63X oil immersion lens. The immunofluorescence signal was quantified on 100 cells using ImageJ software.

#### **In situ proximity ligation assay**

The proximity ligation assay (PLA) was performed by Duolink<sup>®</sup> In Situ Red Starter Kit Mouse/Rabbit (Sigma-Aldrich, Cat # DUO92101) following the manufacturer's protocol. Cells were seeded on round coverslips, fixed with 4% paraformaldehyde, and permeabilized with 0.01% Triton-x and blocked with blocking buffer. The coverslips were incubated for 1 h with different pairs of primary antibodies. The secondary antibody-nucleic acid conjugates PLUS and MINUS were added and were incubated for 1 h at 37 °C. The incubation with ligation mix was done at 37 °C for 30 min followed by amplification with polymerase at 37 °C for 100 min. The coverslips were washed and mounted in microscope slides using mounting medium with DAPI. The PLA signal was indicated as red fluorescent spots using an AxioObserver.Z1 fluorescence microscope (Zeiss, Germany). The number of PLA signal per cell was quantified in 50 cells per sample using ImageJ.

#### **Neutral comet assay**

The detection of DNA double-strand breaks was done using comet assay kit (Trevigen, Cat # 4250-050-K) following the manufacturer's instructions [65]. After treatment, cells were harvested and mixed with low-melting point agarose at 1:100 ratio and transferred to CometSlide. After lysis, the electrophoresis was conducted at 1 V/cm for 50 min. Slides were stained with SYBR gold (Invitrogen, Cat # S11494) for 30 min and visualized by confocal microscope (Nikon, Japan) using FITC filter. The length and intensity of stained DNA tails was calculated by tail moment using ImageJ software.

#### **Clonogenic cell survival assay**

The cell viability after irradiation or DOX treatment was analyzed by colony formation assay. The CBP siRNA transfected cells were seeded in a 6-well plate at low density in triplicates followed by 0.001–1 μM treatment of DOX. For irradiation, the cells were treated with KU55933 or ICI 182780 followed by irradiation. The colonies were fixed after 3 weeks with 70% ethanol for 30 min followed by staining with 1% crystal violet for 5 min. The number of colonies was counted for calculating the plating efficiency and surviving fraction at each dose of irradiation or DOX.

#### **Immunohistochemistry**

Formalin-fixed paraffin-embedded (FFPE) specimens were obtained from breast cancer patients primarily diagnosed with invasive breast carcinoma at the Section of

Translational Surgical Oncology and Biobanking, Department of Surgery, University Medical Center Schleswig–Holstein–Lübeck–Germany, adhering to the guidelines of the local ethical review board (#08–012). Deparaffinization of slides was done by incubation with xylene followed by rehydration in a series of ethanol. Subsequently, the antigen retrieval was carried out by heating the sections in citrate buffer and the endogenous peroxidase was blocked by 3% hydrogen peroxide. The slides were washed 3 times with PBS and blocked with goat serum for 45 min. Anti-CBP and anti-phospho-ATM antibodies were added to tissue sections and incubated at 4 °C overnight. On the next day, the slides were incubated with secondary antibody labeled with biotin for 30 min. After washing with PBS, the addition of diaminobenzidine substrate in combination with avidin–peroxidase complex solution was done. At the end, the slides were stained with hematoxylin and covered with aquatex and scanned by digital microscopy. Immunopositivity of CBP and p-ATM was assessed semi-quantitatively by a consultant histopathologist. The intensity of staining was scored as follows: 0: no staining, 1: weakly positive, 2: moderately positive and 3: strongly positive [66].

### Statistical analyses

Data are presented as the means  $\pm$  standard error of the mean (SEM) of at least three to four independent experiments. The statistical significance was calculated by Mann–Whitney *U* test or two-tailed unpaired Student *t* test using GraphPad Prism 8. The linear regression and Pearson's correlation coefficient (*r*) was calculated using GraphPad Prism 8. The statistical significance was denoted as \*  $P < 0.05$ .

### Supplementary Information

The online version contains supplementary material available at <https://doi.org/10.1186/s13059-025-03528-3>.

Additional file 1: Fig. S1. CBP protein level is stabilized under DNA damage induction. Fig. S2. Analysis of CBP interactions with DNA damage response proteins. Fig. S3. DNA repair efficiency after DNA damage induction in CBP-depleted T47D and MCF7 cells. Fig. S4. Screening of CBP and ATM expression in different CBP knockout clones. Fig. S5. CBP knockout cells are sensitive to DNA damaging agents and are defective in DNA repair. Fig. S6. Phosphorylation of ATM/Chk2 and ATR/Chk1 axis under DNA damage in MDA-MB-231 and MCF7 cells after CBP depletion. Fig. S7. DNA double strand breaks repair efficiency in T47D and SKX cells after CBP downregulation. Fig. S8. ER-independent role of CBP in the response of T47D cells to Etoposide-induced DNA damage. Fig. S9. Involvement of CBP in DNA damage response in lung cancer A549 cells. Fig. S10. Stability and recruitment of NBS1 in CBP-depleted cells after DNA damage induction. Fig. S11. Interaction between CBP and ATM after DNA damage induction in MCF7, T47D and BT-549 cells. Fig. S12. Inhibition of CBP histone acetyltransferase activity reduces the DNA damage response in T47D cells. Fig. S13. Uncropped blots

Additional file 2. Review history

### Acknowledgements

Not applicable.

### Peer review information

Andrew Cosgrove was the primary editor of this article and managed its editorial process and peer review in collaboration with the rest of the editorial team.

### Review history

The review history is available as Additional file 2.

### Authors' contributions

WR, WM, and RA contributed to conception and design of the study; WR, SA, IT, TG, LL, and SM performed experiments and analyzed the data; SA and IT provide acquisition and analysis of data and statistical analysis; WR, WM, and RA contributed to writing and editing of the manuscript; WR, WM, and RA provide funding acquisition. All authors read and approved the final manuscript.

**Funding**

This work was financially supported by generous grants from the King Hussein Award for Cancer Research (grant number 2021-KHA-001) and BMBF grants (grant number 02NUK032& 02NUK035B).

**Data availability**

All data generated or analyzed during this study are included in this published article [and its supplementary information files]. Microscopic immunofluorescence images are available on Figshare (<https://doi.org/10.6084/m9.figshare.28365380>) [67].

**Declarations****Ethics approval and consent to participate**

The formalin-fixed paraffin-embedded (FFPE) specimens were obtained at the Section of Translational Surgical Oncology and Biobanking, Department of Surgery, University Medical Center Schleswig–Holstein–Lübeck–Germany, adhering to the guidelines of the local ethical review board (#08-012). The experimental methods comply with the Helsinki Declaration.

**Consent for publication**

Not applicable

**Competing interests**

The authors declare that they have no competing interests.

**Author details**

<sup>1</sup>Research Institute for Medical and Health Sciences, University of Sharjah, Sharjah, United Arab Emirates. <sup>2</sup>College of Medicine, University of Sharjah, Sharjah, United Arab Emirates. <sup>3</sup>School of Biosciences and Chemistry, Biomolecular Sciences Research Centre, Sheffield Hallam University, Sheffield, UK. <sup>4</sup>Section for Translational Surgical Oncology and Biobanking, Department of Surgery, University of Lübeck and University Hospital Schleswig-Holstein, Lübeck, Germany. <sup>5</sup>Department of Radiotherapy and Radiation Oncology, University Medical Center Hamburg-Eppendorf, Hamburg, Germany. <sup>6</sup>Mildred Scheel Cancer Career Center, HaTriCS4 Program, University Medical Center Hamburg-Eppendorf, Hamburg, Germany. <sup>7</sup>II. Medical Clinic and Polyclinic, University Medical Center Hamburg-Eppendorf, Hamburg, Germany. <sup>8</sup>College of Pharmacy, University of Sharjah, Sharjah, United Arab Emirates.

Received: 22 April 2024 Accepted: 5 March 2025

Published online: 08 April 2025

**References**

1. Veleghzhaninov IO, Ilevlev VA, Pylina YI, Shadrin DM, Vakhrusheva OM. Programming of cell resistance to genotoxic and oxidative stress. *Biomedicines*. 2018;6(1):5. <https://doi.org/10.3390/biomedicines6010005>.
2. Yao Y, Dai W. Genomic instability and cancer. *J Carcinog Mutagen*. 2014;5. <https://doi.org/10.4172/2157-2518.1000165>.
3. Huen MS, Chen J. The DNA damage response pathways: at the crossroad of protein modifications. *Cell Res*. 2008;18(1):8–16. <https://doi.org/10.1038/cr.2007.109>.
4. Helena JM, Joubert AM, Grobbelaar S, Nolte EM, Nel M, Pepper MS et al. Deoxyribonucleic acid damage and repair: capitalizing on our understanding of the mechanisms of maintaining genomic integrity for therapeutic purposes. *Int J Mol Sci*. 2018;19(4). <https://doi.org/10.3390/ijms19041148>.
5. Giglia-Mari G, Zotter A, Vermeulen W. DNA damage response. *Cold Spring Harb Perspect Biol*. 2011;3(1):a000745. <https://doi.org/10.1101/cshperspect.a000745>.
6. Cerosaletti K, Concannon P. Independent roles for nibrin and Mre11–Rad50 in the activation and function of Atm. *J Biol Chem*. 2004;279(37):38813–9. <https://doi.org/10.1074/jbc.M404294200>.
7. Uziel T, Lerenthal Y, Moyal L, Andegeko Y, Mittelman L, Shiloh Y. Requirement of the MRN complex for ATM activation by DNA damage. *EMBO J*. 2003;22(20):5612–21. <https://doi.org/10.1093/emboj/cdg541>.
8. Sun Y, Jiang X, Chen S, Fernandes N, Price BD. A role for the Tip60 histone acetyltransferase in the acetylation and activation of ATM. *Proc Natl Acad Sci USA*. 2005;102(37):13182. <https://doi.org/10.1073/pnas.0504211102>.
9. Sun Y, Jiang X, Price BD. Tip60: connecting chromatin to DNA damage signaling. *Cell Cycle*. 2010;9(5):930–6. <https://doi.org/10.4161/cc.9.5.10931>.
10. Jang ER, Choi JD, Jeong G, Lee JS. Phosphorylation of p300 by ATM controls the stability of NBS1. *Biochem Biophys Res Commun*. 2010;397(4):637–43. <https://doi.org/10.1016/j.bbrc.2010.05.060>.
11. Tang M, Li Z, Zhang C, Lu X, Tu B, Cao Z, et al. SIRT7-mediated ATM deacetylation is essential for its deactivation and DNA damage repair. *Science Advances*. 2019;5(3):eaav1118. <https://doi.org/10.1126/sciadv.aav1118>.
12. Li S, Shi B, Liu X, An HX. Acetylation and deacetylation of DNA repair proteins in cancers. *Front Oncol*. 2020;10. <https://doi.org/10.3389/fonc.2020.573502>.
13. Legube G, Trouche D. Regulating histone acetyltransferases and deacetylases. *EMBO Rep*. 2003;4(10):944–7. <https://doi.org/10.1038/sj.embor.embor941>.
14. Ramadan WS, Talaat IM, Hachim MY, Lischka A, Gemoll T, El-Awady R. The impact of CBP expression in estrogen receptor-positive breast cancer. *Clin Epigenetics*. 2021;13(1):72. <https://doi.org/10.1186/s13148-021-01060-2>.
15. Guo W, Lu J, Dai M, Wu T, Yu Z, Wang J, et al. Transcriptional coactivator CBP upregulates hTERT expression and tumor growth and predicts poor prognosis in human lung cancers. *Oncotarget*. 2014;5(19):9349–61. <https://doi.org/10.18632/oncotarget.2430>.

16. Ward R, Johnson M, Shridhar V, van Deursen J, Couch FJ. CBP truncating mutations in ovarian cancer. *J Med Genet*. 2005;42(6):514–8. <https://doi.org/10.1136/jmg.2004.025080>.
17. Crowley JA, Wang Y, Rapoport AP, Ning Y. Detection of MOZ-CBP fusion in acute myeloid leukemia with 8;16 translocation. *Leukemia*. 2005;19(12):2344–5. <https://doi.org/10.1038/sj.leu.2403971>.
18. Ishihama K, Yamakawa M, Semba S, Takeda H, Kawata S, Kimura S, et al. Expression of HDAC1 and CBP/p300 in human colorectal carcinomas. *J Clin Pathol*. 2007;60(11):1205–10. <https://doi.org/10.1136/jcp.2005.029165>.
19. Oike T, Komachi M, Ogiwara H, Amornwichee N, Saitoh Y, Torikai K, et al. C646, a selective small molecule inhibitor of histone acetyltransferase p300, radiosensitizes lung cancer cells by enhancing mitotic catastrophe. *Radiother Oncol : J Eur Soc Ther Radiol Oncol*. 2014;111(2):222–7. <https://doi.org/10.1016/j.radonc.2014.03.015>.
20. Yan G, Eller MS, Elm C, Larocca CA, Ryu B, Panova IP, et al. Selective inhibition of p300 HAT blocks cell cycle progression, induces cellular senescence, and inhibits the DNA damage response in melanoma cells. *J Invest Dermatol*. 2013;133(10):2444–52. <https://doi.org/10.1038/jid.2013.187>.
21. Tang Z, Yu W, Zhang C, Zhao S, Yu Z, Xiao X, et al. CREB-binding protein regulates lung cancer growth by targeting MAPK and CPSF4 signaling pathway. *Mol Oncol*. 2016;10(2):317–29. <https://doi.org/10.1016/j.molonc.2015.10.015>.
22. Dutto I, Scalera C, Proserpi E. CREBBP and p300 lysine acetyl transferases in the DNA damage response. *Cell Mol Life Sci*. 2018;75(8):1325–38. <https://doi.org/10.1007/s00018-017-2717-4>.
23. Ogiwara H, Ui A, Otsuka A, Satoh H, Yokomi I, Nakajima S, et al. Histone acetylation by CBP and p300 at double-strand break sites facilitates SWI/SNF chromatin remodeling and the recruitment of non-homologous end joining factors. *Oncogene*. 2011;30(18):2135–46. <https://doi.org/10.1038/onc.2010.592>.
24. Cazzalini O, Sommatiss S, Tillhon M, Dutto I, Bachi A, Rapp A, et al. CBP and p300 acetylate PCNA to link its degradation with nucleotide excision repair synthesis. *Nucleic Acids Res*. 2014;42(13):8433–48. <https://doi.org/10.1093/nar/gku533>.
25. Ogiwara H, Kohno T. CBP and p300 histone acetyltransferases contribute to homologous recombination by transcriptionally activating the BRCA1 and RAD51 genes. *PLoS ONE*. 2012;7(12):e52810. <https://doi.org/10.1371/journal.pone.0052810>.
26. Polo SE, Jackson SP. Dynamics of DNA damage response proteins at DNA breaks: a focus on protein modifications. *Genes Dev*. 2011;25(5):409–33. <https://doi.org/10.1101/gad.2021311>.
27. Manickavinayagam S, Velez-Cruz R, Biswas AK, Bedford E, Klein BJ, Kutateladze TG, et al. E2F1 acetylation directs p300/CBP-mediated histone acetylation at DNA double-strand breaks to facilitate repair. *Nat Commun*. 2019;10(1):4951. <https://doi.org/10.1038/s41467-019-12861-8>.
28. Söderberg O, Gullberg M, Jarvius M, Ridderstråle K, Leuchowius KJ, Jarvius J, et al. Direct observation of individual endogenous protein complexes in situ by proximity ligation. *Nat Methods*. 2006;3(12):995–1000. <https://doi.org/10.1038/nmeth947>.
29. Ogiwara H, Sasaki M, Mitachi T, Oike T, Higuchi S, Tominaga Y, et al. Targeting p300 addiction in CBP-deficient cancers causes synthetic lethality by apoptotic cell death due to abrogation of MYC expression. *Cancer Discov*. 2016;6(4):430–45. <https://doi.org/10.1158/2159-8290.Cd-15-0754>.
30. García-Santisteban I, Llopis A, Krenning L, Vallejo-Rodríguez J, van den Broek B, Zubiaga AM, et al. Sustained CHK2 activity, but not ATM activity, is critical to maintain a G1 arrest after DNA damage in untransformed cells. *BMC Biol*. 2021;19(1):35. <https://doi.org/10.1186/s12915-021-00965-x>.
31. Mansour WY, Bogdanova NV, Kasten-Pisula U, Rieckmann T, Köcher S, Borgmann K, et al. Aberrant overexpression of miR-421 downregulates ATM and leads to a pronounced DSB repair defect and clinical hypersensitivity in SKX squamous cell carcinoma. *Radiother Oncol*. 2013;106(1):147–54. <https://doi.org/10.1016/j.radonc.2012.10.020>.
32. Smith CL, Onate SA, Tsai MJ, O'Malley BW. CREB binding protein acts synergistically with steroid receptor coactivator-1 to enhance steroid receptor-dependent transcription. *Proc Natl Acad Sci U S A*. 1996;93(17):8884–8. <https://doi.org/10.1073/pnas.93.17.8884>.
33. Acevedo ML, Kraus WL. Mediator and p300/CBP-steroid receptor coactivator complexes have distinct roles, but function synergistically, during estrogen receptor alpha-dependent transcription with chromatin templates. *Mol Cell Biol*. 2003;23(1):335–48. <https://doi.org/10.1128/mcb.23.1.335-348.2003>.
34. Chen H, Lin RJ, Xie W, Wilpitz D, Evans RM. Regulation of hormone-induced histone hyperacetylation and gene activation via acetylation of an acetylase. *Cell*. 1999;98(5):675–86. [https://doi.org/10.1016/s0092-8674\(00\)80054-9](https://doi.org/10.1016/s0092-8674(00)80054-9).
35. Rouzier R, Perou CM, Symmans WF, Ibrahim N, Cristofanilli M, Anderson K, et al. Breast cancer molecular subtypes respond differently to preoperative chemotherapy. *Clin Cancer Res*. 2005;11(16):5678–85. <https://doi.org/10.1158/1078-0432.ccr-04-2421>.
36. Kim SI, Sohn J, Koo JS, Park SH, Park HS, Park BW. Molecular subtypes and tumor response to neoadjuvant chemotherapy in patients with locally advanced breast cancer. *Oncology*. 2010;79(5–6):324–30. <https://doi.org/10.1159/000322192>.
37. Jang ER, Choi JD, Lee JS. Acetyltransferase p300 regulates NBS1-mediated DNA damage response. *FEBS Lett*. 2011;585(1):47–52. <https://doi.org/10.1016/j.febslet.2010.11.034>.
38. You Z, Chahwan C, Bailis J, Hunter T, Russell P. ATM activation and its recruitment to damaged DNA require binding to the C terminus of Nbs1. *Mol Cell Biol*. 2005;25(13):5363–79. <https://doi.org/10.1128/mcb.25.13.5363-5379.2005>.
39. Watters D, Kedar P, Spring K, Bjorkman J, Chen P, Gatei M, et al. Localization of a portion of extranuclear ATM to peroxisomes. *J Biol Chem*. 1999;274(48):34277–82. <https://doi.org/10.1074/jbc.274.48.34277>.
40. Kozlov SV, Waardenberg AJ, Engholm-Keller K, Arthur JW, Graham ME, Lavin M. Reactive Oxygen Species (ROS)-activated ATM-dependent phosphorylation of cytoplasmic substrates identified by large-scale phosphoproteomics screen. *Mol Cell Proteomics*. 2016;15(3):1032–47. <https://doi.org/10.1074/mcp.M115.055723>.
41. Morita A, Tanimoto K, Murakami T, Morinaga T, Hosoi Y. Mitochondria are required for ATM activation by extranuclear oxidative stress in cultured human hepatoblastoma cell line Hep G2 cells. *Biochem Biophys Res Commun*. 2014;443(4):1286–90. <https://doi.org/10.1016/j.bbrc.2013.12.139>.
42. Xu W, Zhao S. Generation and characterization of pan-specific anti-acetyllysine antibody. *Methods Mol Biol (Clifton, NJ)*. 2013;981:137–50. [https://doi.org/10.1007/978-1-62703-305-3\\_11](https://doi.org/10.1007/978-1-62703-305-3_11).

43. Sun Y, Xu Y, Roy K, Price BD. DNA damage-induced acetylation of lysine 3016 of ATM activates ATM kinase activity. *Mol Cell Biol*. 2007;27(24):8502–9. <https://doi.org/10.1128/MCB.01382-07>.
44. Kramer D, Schön M, Bayerlová M, Bleckmann A, Schön MP, Zörnig M, et al. A pro-apoptotic function of IASPP by stabilizing p300 and CBP through inhibition of BRMS1 E3 ubiquitin ligase activity. *Cell Death Dis*. 2015;6(2):e1634-e. <https://doi.org/10.1038/cddis.2015.17>.
45. Nagasaka M, Miyajima C, Aoki H, Aoyama M, Morishita D, Inoue Y, et al. Insights into regulators of p53 Acetylation. *Cells*. 2022;11(23):3825. <https://doi.org/10.3390/cells11233825>.
46. Schaffner C, Stilgenbauer S, Rappold GA, Döhner H, Lichter P. Somatic ATM mutations indicate a pathogenic role of ATM in B-cell chronic lymphocytic leukemia. *Blood*. 1999;94(2):748–53.
47. Laake K, Jansen L, Hahnemann JM, Brondum-Nielsen K, Lönnqvist T, Kääriäinen H, et al. Characterization of ATM mutations in 41 Nordic families with ataxia telangiectasia. *Hum Mutat*. 2000;16(3):232–46. [https://doi.org/10.1002/1098-1004\(200009\)16:3%3c232::Aid-humu6%3e3.0.Co;2-l](https://doi.org/10.1002/1098-1004(200009)16:3%3c232::Aid-humu6%3e3.0.Co;2-l).
48. Chen Y, Wu J, Zhai L, Zhang T, Yin H, Gao H, et al. Metabolic regulation of homologous recombination repair by MRE11 lactylation. *Cell*. 2024;187(2):294–311.e21. <https://doi.org/10.1016/j.cell.2023.11.022>.
49. Chiu LY, Gong F, Miller KM. Bromodomain proteins: repairing DNA damage within chromatin. *Philos Trans R Soc Lond B Biol Sci*. 2017;372(1731):20160286. <https://doi.org/10.1098/rstb.2016.0286>.
50. Sardar S, McNair CM, Ravindranath L, Chand SN, Yuan W, Bogdan D, et al. AR coactivators, CBP/p300, are critical mediators of DNA repair in prostate cancer. *Oncogene*. 2024;43(43):3197–213. <https://doi.org/10.1038/s41388-024-03148-4>.
51. Chen J, Zhu F, Weeks RL, Biswas AK, Guo R, Li Y, et al. E2F1 promotes the recruitment of DNA repair factors to sites of DNA double-strand breaks. *Cell Cycle*. 2011;10(8):1287–94. <https://doi.org/10.4161/cc.10.8.15341>.
52. Lin WC, Lin FT, Nevins JR. Selective induction of E2F1 in response to DNA damage, mediated by ATM-dependent phosphorylation. *Genes Dev*. 2001;15(14):1833–44.
53. Adamowicz M. Breaking up with ATM. *J Immunol Sci*. 2018;2(1):26–31.
54. So S, Davis AJ, Chen DJ. Autophosphorylation at serine 1981 stabilizes ATM at DNA damage sites. *J Cell Biol*. 2009;187(7):977–90. <https://doi.org/10.1083/jcb.200906064>.
55. Kühne M, Riballo E, Rief N, Rothkamm K, Jeggo PA, Löbrich M. A double-strand break repair defect in ATM-deficient cells contributes to radiosensitivity. *Can Res*. 2004;64(2):500–8. <https://doi.org/10.1158/0008-5472.Can-03-2384>.
56. Park JH, Park EJ, Lee HS, Kim SJ, Hur SK, Imbalzano AN, et al. Mammalian SWI/SNF complexes facilitate DNA double-strand break repair by promoting gamma-H2AX induction. *Embo j*. 2006;25(17):3986–97. <https://doi.org/10.1038/sj.emboj.7601291>.
57. Kwon SJ, Park JH, Park EJ, Lee SA, Lee HS, Kang SW, et al. ATM-mediated phosphorylation of the chromatin remodeling enzyme BRG1 modulates DNA double-strand break repair. *Oncogene*. 2015;34(3):303–13. <https://doi.org/10.1038/ncr.2013.556>.
58. Guo X, Yang C, Qian X, Lei T, Li Y, Shen H, et al. Estrogen receptor  $\alpha$  regulates ATM Expression through miRNAs in breast cancer. *Clin Cancer Res*. 2013;19(18):4994–5002. <https://doi.org/10.1158/1078-0432.Ccr-12-3700>.
59. Kwok RP, Lundblad JR, Chrivia JC, Richards JP, Bächinger HP, Brennan RG, et al. Nuclear protein CBP is a coactivator for the transcription factor CREB. *Nature*. 1994;370(6486):223–6. <https://doi.org/10.1038/370223a0>.
60. Kasten-Pisula U, Menegakis A, Brammer I, Borgmann K, Mansour WY, Degenhardt S, et al. The extreme radiosensitivity of the squamous cell carcinoma SKX is due to a defect in double-strand break repair. *Radiother Oncol*. 2009;90(2):257–64. <https://doi.org/10.1016/j.radonc.2008.10.019>.
61. Ramadan WS, Vazhappilly CG, Saleh EM, Menon V, AlAzawi AM, El-Serafi AT et al. Interplay between epigenetics, expression of estrogen receptor-  $\alpha$ , HER2/ERBB2 and sensitivity of triple negative breast cancer cells to hormonal therapy. *Cancers (Basel)*. 2018;11(1). <https://doi.org/10.3390/cancers11010013>.
62. Cubillos-Rojas M, Amair-Pinedo F, Tato I, Bartrons R, Ventura F, Rosa JL. Tris-acetate polyacrylamide gradient gels for the simultaneous electrophoretic analysis of proteins of very high and low molecular mass. *Methods Mol Biol (Clifton, NJ)*. 2012;869:205–13. [https://doi.org/10.1007/978-1-61779-821-4\\_17](https://doi.org/10.1007/978-1-61779-821-4_17).
63. El-Awady RA, Hersi F, Al-Tunajji H, Saleh EM, Abdel-Wahab AH, Al Homssi A, et al. Epigenetics and miRNA as predictive markers and targets for lung cancer chemotherapy. *Cancer Biol Ther*. 2015;16(7):1056–70. <https://doi.org/10.1080/15384047.2015.1046023>.
64. Elsesy ME, Oh-Hohenhorst SJ, Löser A, Qing C, Mutiara S, Köcher S, et al. Second-generation antiandrogen therapy radiosensitizes prostate cancer regardless of castration state through inhibition of DNA double strand break repair. *Cancers*. 2020;12(9):2467. <https://doi.org/10.3390/cancers12092467>.
65. Lozon L, Saleh E, Menon V, Ramadan WS, Amin A, El-Awady R. Effect of safranal on the response of cancer cells to topoisomerase I inhibitors: does sequence matter? *Front Pharmacol*. 2022;13:938471. <https://doi.org/10.3389/fphar.2022.938471>.
66. Diallo-Danebrock R, Ting E, Gluz O, Herr A, Mohrmann S, Geddert H, et al. Protein expression profiling in high-risk breast cancer patients treated with high-dose or conventional dose-dense chemotherapy. *Clin Cancer Res*. 2007;13(2 Pt 1):488–97. <https://doi.org/10.1158/1078-0432.ccr-06-1842>.
67. Ramadan WAS, Talaat I, Lozon L, Mouffak S, Gemoll T, Mansour W, El-Awady R. The histone acetyltransferase CBP participates in regulating the DNA damage response through ATM after double strand breaks. *Microscopic immunofluorescence images Figshare*. 2025. <https://doi.org/10.6084/m9.figshare.28365380>.

## Publisher's Note

Springer Nature remains neutral with regard to jurisdictional claims in published maps and institutional affiliations.